Light axial vector mesons

Kan Chen, Cheng-Qun Pang, Xiang Liu, and Takayuki Matsuki

Phys. Rev. D **91**, 074025 — Published 22 April 2015

DOI: 10.1103/PhysRevD.91.074025

Light axial vector mesons

Kan Chen[1,2],* Cheng-Qun Pang[1,2],† Xiang Liu[1,2‡],§ and Takayuki Matsuki[3,4,1¶]
[1]*School of Physical Science and Technology, Lanzhou University, Lanzhou 730000, China*
[2]*Research Center for Hadron and CSR Physics, Lanzhou University & Institute of Modern Physics of CAS, Lanzhou 730000, China*
[3]*Tokyo Kasei University, 1-18-1 Kaga, Itabashi, Tokyo 173-8602, Japan*
[4]*Theoretical Research Division, Nishina Center, RIKEN, Saitama 351-0198, Japan*

Inspired by the abundant experimental observation of axial vector states, we study whether the observed axial vector states can be categorized into the conventional axial vector meson family. In this paper we carry out analysis based on the mass spectra and two-body Okubo-Zweig-Iizuka-allowed decays. Besides testing the possible axial vector meson assignments, we also predict abundant information for their decays and the properties of some missing axial vector mesons, which are valuable to further experimental exploration of the observed and predicted axial vector mesons.

PACS numbers: 14.40.Be, 12.38.Lg, 13.25.Jx

I. INTRODUCTION

Among the light unflavored mesons listed in Particle Data Group (PDG) [1], there are abundant light axial vector mesons with a spin-parity quantum number $J^P = 1^+$, which form a P-wave meson family. Usually, we adopt h_1, b_1, f_1, and a_1 to express the corresponding states with the quantum numbers, $I^G(J^{PC}) = 0^-(1^{+-})$, $1^+(1^{+-})$, $0^+(1^{++})$, and $1^-(1^{++})$, respectively. In Table I, we collect the experimental information of the observed h_1, b_1, f_1, and a_1 states, which includes the corresponding resonance parameters and these observed decay channels.

Facing so many axial vector states in PDG, we need to examine whether all these states can be categorized into the axial vector meson family, which is crucial to reveal their underlying structures. We also notice that most axial vector states are either omitted by PDG or are recent findings needing confirmation. Just because of unclear experimental status of light axial vector states, we need to carry out a quantitative investigation of them, which is helpful to further experimental study, especially for these axial vector states either omitted by PDG or unconfirmed by other experiments.

In this work, we carry out a systematic study of the axial vector states by analyzing mass spectra and Okubo-Zweig-Iizuka (OZI)-allowed two-body strong decay behaviors. Our investigations are based on the assumption that all the axial mesons can be explained within the conventional $q\bar{q}$ picture. Comparing our numerical results with the experimental data, we can further test the possible assignments of the states in the axial vector meson family. In addition, information of the predicted decays of the axial vector states observed or still missing in experiment is valuable to further experimental study of axial vector meson.

This paper is organized as follows. After Introduction, we present the phenomenological analysis by combining our theoretical results with the corresponding experimental data in Sec. II, where the Regge trajectory analysis is adopted to study mass spectra of the axial vector meson family and the quark pair creation (QPC) model is applied to calculate their OZI-allowed strong decay behavior. Finally, the discussion and conclusion are given in Sec. III.

II. PHENOMENOLOGICAL STUDY OF OBSERVED AXIAL VECTOR STATES

A Regge trajectory analysis is an effective approach to study a meson spectrum [31], especially to a light meson spectrum. Masses and radial quantum numbers of light mesons with the same quantum number satisfy the following relation

$$M^2 = M_0^2 + (n-1)\mu^2, \tag{1}$$

where M_0 and M are the masses of a ground state and the corresponding radial excitation with a radial quantum number n, respectively. μ^2 denotes a slope of a trajectory with a universal $\mu^2 = 1.25 \pm 0.15\ \mathrm{GeV}^2$ [31].

In Fig. 1, we present the Regge trajectory analysis, in which we consider all the axial vector states listed in PDG as shown in Table I. Besides the observed ones, we also predict some missing states and show them in Fig. 1. Additionally, we notice that there are two possible candidates for the a_1 meson with quantum number $n^{2s+1}J_L = 3^3P_1$, i.e., the $a_1(1930)$ and $a_1(2095)$. On the other hand, both the $f_1(1420)$ and $f_1(1510)$ can be an $s\bar{s}$ partner of the $f_1(1285)$ by anaylyzing only the Regge trajectory. Thus, a further study of their strong decay behaviors is helpful to test these possible assignments to the observed axial vector states and can provides more predictions of the observed and still missing axial vector mesons, which are valuable to future experimental exploration of axial vector mesons.

To obtain the decay behaviors of the axial vector mesons, we adopt the quark pair creation (QPC) model, which was first proposed by Micu [32], and further developed by the Orsay group [33–37]. This model was widely applied to study the OZI-allowed two-body strong decay of hadrons [38–59]. In the following, we briefly introduce the QPC model.

‡Corresponding author
*Electronic address: chenk_10@lzu.edu.cn
†Electronic address: pangchq13@lzu.edu.cn
§Electronic address: xiangliu@lzu.edu.cn
¶Electronic address: matsuki@tokyo-kasei.ac.jp

TABLE I: Resonance parameters and strong decay channels of the axial vector states collected in PDG [1]. The mass and width are average values taken from PDG. The states omitted from PDG summary table are marked by a superscript ♮, while the states listed as further states in PDG are marked by a superscript ♭.

$I^G(J^{PC})$	State	Mass (MeV)	Width (MeV)	The observed decay channels
	$a_1(1260)$	1230 ± 40	$250 \sim 600$	3π [2], $\pi\rho$ [3], $\sigma\pi$ [4]
	$a_1(1640)^\natural$	1647 ± 22	254 ± 27	3π [5], $\pi\rho$ [4, 6] , $\sigma\pi$ [5], $f_2(1270)\pi$ [5]
$1^-(1^{++})$	$a_1(1930)^\flat$	1930^{+30}_{-70}	155 ± 45	$3\pi^0$ [7]
	$a_1(2095)^\flat$	$2096 \pm 17 \pm 121$	$451 \pm 41 \pm 81$	$\pi^+\pi^-\pi^-$ [8]
	$a_1(2270)^\flat$	2270^{+55}_{-40}	305^{+70}_{-40}	$3\pi^0$ [7]
	$b_1(1235)$	1229.5 ± 3.2	142 ± 9	$\omega\pi$ [9–11]
$1^+(1^{+-})$	$b_1(1960)^\flat$	1960 ± 35	345 ± 75	$\omega\pi^0$ [12]
	$b_1(2240)^\flat$	2240 ± 35	320 ± 85	$\omega\pi^0$[12]
	$f_1(1285)$	1282.1 ± 0.6	24.2 ± 1.1	$\rho^0\rho^0$ [13], $\eta\pi\pi$ [14–16], $a_0\pi$ [15–17], $K\bar{K}\pi$ [15, 16, 18]
	$f_1(1420)$	1426.4 ± 0.9	54.9 ± 2.6	$K\bar{K}\pi$ [19, 20], $K\bar{K}^*(892) + c.c$ [18–20]
$0^+(1^{++})$	$f_1(1510)^\natural$	1518 ± 5	73 ± 25	$K\bar{K}^*(892) + c.c$ [21, 22], $\pi^+\pi^-\eta'$[23]
	$f_1(1970)^\flat$	1971 ± 15	240 ± 45	$\eta\pi^0\pi^0$ [24]
	$f_1(2310)^\flat$	2310 ± 60	255 ± 70	$\eta\pi^0\pi^0$ [24]
	$h_1(1170)$	1170 ± 20	360 ± 40	$\pi\rho$ [25–27]
	$h_1(1380)^\natural$	1386 ± 19	91 ± 30	$K\bar{K}^*(892) + c.c$ [21, 28]
$0^-(1^{+-})$	$h_1(1595)^\natural$	$1594 \pm 15^{+10}_{-60}$	$384 \pm 60^{+70}_{100}$	$\omega\eta$ [29]
	$h_1(1965)^\flat$	1965 ± 45	345 ± 75	$\omega\eta$ [30]
	$h_1(2215)^\flat$	2215 ± 40	325 ± 55	$\omega\eta$ [30]

For a decay process $A \to B + C$, we can write out

$$\langle BC|\mathcal{T}|A\rangle = \delta^3(\mathbf{P}_B + \mathbf{P}_C)\mathcal{M}^{M_{J_A}M_{J_B}M_{J_C}}, \tag{2}$$

where $\mathbf{P}_{B(C)}$ is a three-momentum of a meson $B(C)$ in the rest frame of a meson A. A subscript M_{J_i} $(i = A, B, C)$ denotes an orbital magnetic momentum. The transition operator $\mathcal{T}$ is introduced to describe a quark-antiquark pair creation from vacuum, which has a quantum number $J^{PC} = 0^{++}$, i.e., $\mathcal{T}$ can be expressed as

$$\begin{aligned}\mathcal{T} &= -3\gamma\sum_m \langle 1m;1\ -m|00\rangle \int d\mathbf{p}_3 d\mathbf{p}_4 \delta^3(\mathbf{p}_3+\mathbf{p}_4) \\ &\times \mathcal{Y}_{1m}\left(\frac{\mathbf{p}_3-\mathbf{p}_4}{2}\right)\chi^{34}_{1,-m}\phi^{34}_0\left(\omega^{34}_0\right)_{ij} b^\dagger_{3i}(\mathbf{p}_3)d^\dagger_{4j}(\mathbf{p}_4),\end{aligned} \tag{3}$$

which is constructed via a completely phenomenological way to reflect a creation of a pair of quark and antiquark from vacuum, where quark and antiquark are denoted by indices 3 and 4, respectively. As a dimensionless parameter, γ depicts the strength of a creation of $q\bar{q}$ from vacuum, where γ is 8.7 and $8.7/\sqrt{3}$ [51] corresponding to the $u\bar{u}/d\bar{d}$ and $s\bar{s}$ creations, respectively. $\mathcal{Y}_{\ell m}(\mathbf{p}) = |\mathbf{p}|^\ell Y_{\ell m}(\mathbf{p})$ is the solid harmonic. χ, ϕ, and ω denote the spin, flavor, and color wave functions, which can be treated separately. In addition, i and j denote the color indices of a $q\bar{q}$ pair.

By the Jacob-wick formula [60], a decay amplitude is expressed as

$$\begin{aligned}\mathcal{M}^{JL}(\mathbf{P}) &= \frac{\sqrt{4\pi(2L+1)}}{2J_A+1}\sum_{M_{J_B}M_{J_C}}\langle L0;JM_{J_A}|J_AM_{J_A}\rangle \\ &\times\langle J_BM_{J_B};J_CM_{J_C}|J_AM_{J_A}\rangle\mathcal{M}^{M_{J_A}M_{J_B}M_{J_C}},\end{aligned} \tag{4}$$

and a general decay width reads as

$$\Gamma = \frac{\pi}{4}\frac{|\mathbf{P}|}{m_A^2}\sum_{J,L}|\mathcal{M}^{JL}(\mathbf{P})|^2, \tag{5}$$

where m_A is the mass of an initial state A. We use the simple harmonic oscillator (SHO) wave function to describe a space wave function of mesons, which has the following expression

$$\Psi_{nlm}(R,\mathbf{p}) = \mathcal{R}_{nl}(R,\mathbf{p})\mathcal{Y}_{lm}(\mathbf{p}), \tag{6}$$

where the concrete values of a parameter R involved in our calculation are given in Ref. [61] for the ground states. However, its value is to be fixed for each excited state.

With the above preparation, we further discuss the OZI-allowed decay behaviors of the axial vector mesons, where the allowed decay modes are listed in Tables II-III.

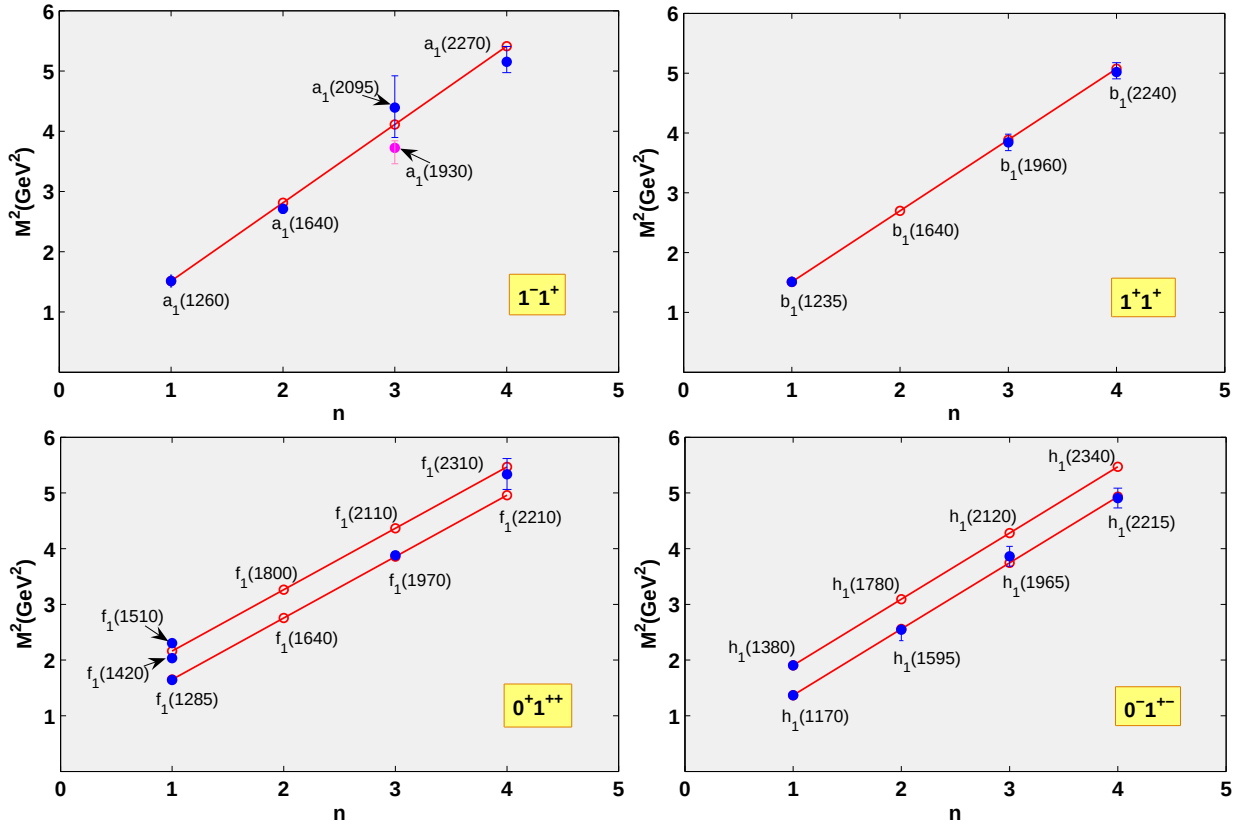

FIG. 1: (color online). Regge trajectory analysis for a_1, b_1, f_1, and h_1 with typical $\mu^2 = 1.30$ GeV^2, 1.19 GeV^2, 1.10 GeV^2, and 1.19 GeV^2, respectively, which can be covered by $\mu^2 = 1.25 \pm 0.15$ GeV^2 given in Ref. [31]. The experimental errors of discussed axial vector states are given, which are taken from PDG [1]. Here, ∘ and • denote theoretical and experimental values, respectively.

A. a_1 states

The Regge trajectory analysis indicates that the $a_1(1260)$ can be regarded as a ground state. The obtained total and partial decay widths of the $a_1(1260)$ are listed in Fig. 2, which shows that $\pi\rho$ is the dominant channel. In Fig. 2, we give the partial decay widths of $a_1(1260) \to \pi\rho$ from the S-wave and D-wave contributions. Here, the D-wave/S-wave amplitude ratio in the decay $a_1(1260) \to \pi\rho$ is -0.248 with a typical value of $R = 3.846$ GeV^{-1} [61] in our calculation, which is comparable with the B852 data $(-0.14 \pm 0.04 \pm 0.07)$ [4]. Our result also shows that $a_1(1260) \to f_0\pi$ is a subordinate decay mode with the partial decay width 1.82 MeV, which explains why there has been no evidence of $a_1(1260) \to f_0\pi$ in experiment [3]. As shown in Fig. 2, the calculated total width can reproduce the CMD2 data given by Ref. [62]. In addition, we also give some typical ratios relevant to the partial decay and total widths together with the corresponding experimental data in Table IV. In summary, our results are comparable with the experimental values and support $a_1(1260)$ as a ground state in the a_1 meson family.

If the $a_1(1640)$ is the first radial excitation of the $a_1(1260)$, its decay behavior depending on the R value is shown in Fig. 3. We use the experimental total width [5] and the ratio $\Gamma(f_2(1270)\pi)/\Gamma(\sigma\pi) = 0.24 \pm 0.07$ [5] to get $R = (4.30 \sim 4.64)$

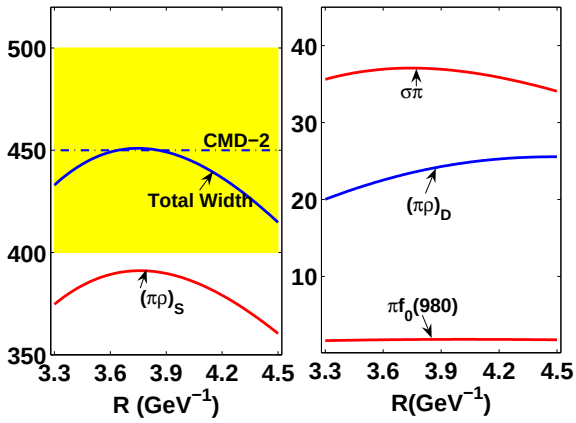

FIG. 2: (color online). Total and partial decay widths of the $a_1(1260)$ depending on R. Here, the dot-dashed line with band is taken from the experimental data in Ref. [62]. The S-wave and D-wave contributions to the decay width of $a_1(1260) \to \pi\rho$ are also given separately. All results are in units of MeV.

TABLE II: OZI-allowed two-body decay channels for a_1 and h_1 states marked by √. Here, ρ, ω, and η denote $\rho(770)$, $\omega(782)$, and $\eta(548)$, respectively. The axial vector states predicted by the Regge trajectory analysis are marked by a superscript ♮.

Channel	$a_1(1260)$	$a_1(1640)$	$a_1(1930)$	$a_1(2095)$	$a_1(2270)$	Channel	$h_1(1170)$	$h_1(1380)$	$h_1(1595)$	$h_1^\natural(1780)$	$h_1(1965)$	$h_1^\natural(2120)$	$h_1(2215)$	$h_1^\natural(2340)$
$\pi\rho$	√	√	√	√	√	$\pi\rho$	√	√	√	√	√	√	√	√
$\sigma\pi$	√	√	√	√	√	KK^*		√	√	√	√	√	√	√
πf_0	√	√	√	√	√	$\eta\omega$		√	√	√	√	√	√	√
$\pi f_1(1420)$		√	√	√	√	$\omega\sigma$			√	√	√	√	√	√
$\pi\rho(1450)$		√	√	√	√	$KK_1(1270)$				√	√	√	√	√
$\rho\omega$		√	√	√	√	$\omega\eta'(958)$				√	√	√	√	√
$\eta a_0(980)$		√	√	√	√	ωf_0				√	√	√	√	√
KK^*		√	√	√	√	$\rho a_0(980)$				√	√	√	√	√
$\pi b_1(1235)$		√	√	√	√	$\pi\rho(1450)$				√	√	√	√	√
$\pi f_2(1270)$		√	√	√	√	$KK_1(1400)$					√	√	√	√
$\pi f_1(1285)$		√	√	√	√	$KK^*(1410)$					√	√	√	√
$\rho a_0(980)$			√	√	√	$KK_0^*(1430)$					√	√	√	√
$KK_1(1400)$			√	√	√	$KK_2^*(1430)$					√	√	√	√
$\eta a_1(1260)$			√	√	√	K^*K^*					√	√	√	√
$\pi\rho(1700)$			√	√	√	$\eta\omega(1420)$					√	√	√	√
$KK_1(1270)$			√	√	√	$\sigma h_1(1170)$					√	√	√	√
$KK^*(1410)$			√	√	√	$\pi\rho(1700)$					√	√	√	√
$KK_0^*(1430)$			√	√	√	$\rho a_2(1320)$						√	√	√
$KK_2^*(1430)$			√	√	√	$\omega f_2(1270)$						√	√	√
K^*K^*			√	√	√	$\sigma\omega(1420)$						√	√	√
$\eta a_2(1320)$			√	√	√	$\omega f_1(1285)$						√	√	√
$\sigma a_1(1260)$			√	√	√	$\rho\pi(1300)$						√	√	√
$\sigma a_2(1320)$			√	√	√	$\rho a_1(1260)$						√	√	√
$\rho\pi(1300)$				√	√	$K^*K_1(1270)$							√	√
$\eta a_0(1450)$				√	√	$f_0h_1(1170)$							√	√
$\omega b_1(1235)$				√	√	$KK^*(1680)$							√	√
$\rho h_1(1170)$				√	√	$\omega f_1(1420)$							√	√
$\rho a_1(1260)$				√	√	$K^*K_1(1400)$								√
$K^*K_1(1270)$					√									
$\rho a_2(1320)$					√									
$\rho\omega(1420)$					√									
$\rho a_0(1450)$					√									
$KK^*(1680)$					√									
$\eta'(958)a_0(980)$					√									

GeV^{-1}[1]. The main decay modes of $a_1(1640)$ are $\pi\rho$, $\pi\rho(1450)$, $\pi f_2(1270)$, $\pi f_1(1285)$, and $\rho\omega$. Additionally, we further provide information of the typical ratios of the $a_1(1640)$ decays in Table V.

There are two possibilities of a candidate of the second radial excitation of the $a_1(1260)$. In the following, we discuss the decay behaviors of the $a_1(1930)$ and $a_1(2095)$ combining the corresponding experimental data. In Figures 4 and 5, we present the R dependence of the decay behaviors of these a_1's, respectively. That is, the obtained total width of the $a_1(1930)$ can be fitted with the data in Ref. [7] when $R = 4.58 \sim 4.92$ GeV^{-1}, while that of $a_1(2095)$ can overlap with the experimental data [7] when $R = (4.78 \sim 5.16)$ GeV^{-1}. Thus, it is difficult to distinguish which a_1 is more

[1] By the experimental total width [5], we find that there exists overlap between our theoretical and experimental results when taking $R = 4.26 \sim 4.92$ GeV^{-1}. Then, we can further constrain the R values by the ratio $\Gamma(f_2(1270)\pi)/\Gamma(\sigma\pi) = 0.24 \pm 0.07$ [5], where the constrained $R = (4.30 \sim 4.64)$ GeV^{-1}, which is adopted to present other typical ratios of $a_1(1640)$.

TABLE III: OZI-allowed two-body decay channels for b_1 and f_1 states marked by √. Here, ρ, ω, and η denote $\rho(770)$, $\omega(782)$, and $\eta(548)$, respectively. The axial vector states predicted by the Regge trajectory analysis are marked by a superscript ♮.

Channel	$b_1(1235)$	$b_1^\natural(1640)$	$b_1(1960)$	$b_1(2240)$	Channel	$f_1(1285)$	$f_1(1420)$	$f_1(1510)$	$f_1^\natural(1640)$	$f_1^\natural(1800)$	$f_1(1970)$	$f_1^\natural(2110)$	$f_1^\natural(2210)$	$f_1(2310)$
$\pi\omega$	√	√	√	√	$\pi a_0(980)$	√	√	√	√	√	√	√	√	√
$\pi a_0(980)$	√	√	√	√	$\sigma\eta$	√	√	√	√	√	√	√	√	√
$\pi a_1(1260)$		√	√	√	$\pi a_1(1260)$		√	√	√	√	√	√	√	√
$\pi a_2(1320)$		√	√	√	KK^*		√	√	√	√	√	√	√	√
$\pi\omega(1420)$		√	√	√	$\pi a_2(1320)$			√	√	√	√	√	√	√
$\pi a_0(1450)$		√	√	√	$\pi a_0(1450)$				√	√	√	√	√	√
$\eta\rho$		√	√	√	ηf_0				√	√	√	√	√	√
$\rho\rho$		√	√	√	$\rho\rho$				√	√	√	√	√	√
KK^*		√	√	√	$\omega\omega$				√	√	√	√	√	√
$\sigma\rho$		√	√	√	$\sigma\eta'$				√	√	√	√	√	√
$\eta'(958)\rho$			√	√	$KK_1(1270)$					√	√	√	√	√
ρf_0			√	√	K^*K^*					√	√	√	√	√
$\omega a_0(980)$			√	√	$\omega h_1(1170)$						√	√	√	√
$KK_1(1270)$			√	√	$\eta'(958)f_0$						√	√	√	√
$KK_1(1400)$			√	√	$\eta f_2(1270)$						√	√	√	√
$KK_0^*(1410)$			√	√	$KK_1(1400)$						√	√	√	√
$KK_0^*(1430)$			√	√	$KK^*(1410)$						√	√	√	√
$KK_2^*(1430)$			√	√	$KK_0^*(1430)$						√	√	√	√
$\sigma b_1(1235)$			√	√	$KK_2^*(1430)$						√	√	√	√
K^*K^*			√	√	$\eta f_1(1285)$						√	√	√	√
$\omega a_2(1320)$				√	$\sigma f_2(1270)$						√	√	√	√
$\omega\pi(1300)$				√	$\sigma f_1(1285)$						√	√	√	√
$K^*K_1(1270)$				√	$\sigma f_1(1420)$							√	√	√
$\eta\rho(1450)$				√	$\rho b_1(1235)$							√	√	√
$KK^*(1680)$				√	$\eta f_1(1420)$							√	√	√
$a_0(980)h_1(1170)$				√	$\omega\omega(1420)$								√	√
$\rho f_2(1270)$				√	$K^*K_1(1270)$								√	√
$\rho f_1(1285)$				√	$KK^*(1680)$									√
$\rho f_1(1420)$				√	$f_0f_2(1270)$									√
$\rho b_1(1235)$				√	$f_0f_1(1285)$									√
$\omega a_1(1260)$				√	$a_0(980)a_1(1260)$									√
					$a_0(980)\pi(1300)$									√
					$a_0(980)a_2(1320)$									√
					$\eta'(958)f_2(1270)$									√
					$\rho\rho(1450)$									√
					$\eta'(958)f_1(1285)$									√
					$K^*K_1(1400)$									√

suitable for a candidate of the second radial excitation of the $a_1(1260)$ by studying only the total decay widths. Besides, we can learn from Regge trajectory analysis that there is only one state for 3^3P_1 state, and it is doubtful that both $a_1(1930)$ and $a_1(2095)$ are exist as mentioned in Ref. [7]. However, there exist different behaviors of the partial decay widths of these a_1's. The $a_1(1930)$ mainly decays into final states $\pi\rho$, $\pi\rho(1450)$, and $\pi b_1(1235)$, while the $\pi f_1(1285)$ and $\sigma\pi$ modes also have sizable contributions. The decays of the $a_1(1930)$ into $KK_0^*(1430)$, $KK_2^*(1430)$, and $K^*(896)K^*(896)$ have tiny decay widths, which are not listed in Fig. 4. As for the $a_1(2095)$, its dominant decay channels are $\pi b_1(1235)$, $\pi\rho$, and $\pi\rho(1450)$ and are shown in Fig. 5. The other decay channels like $\rho a_0(980)$, $\pi\rho(1700)$, $\pi f_1(1285)$, πf_0, and $\sigma\pi$ also have

TABLE IV: Some typical ratios of decay widths of the $a_1(1260)$. The $\Gamma(\pi\rho)_{S(D)}$ represent the $S\,(D)$-wave decay width of $a_1(1260) \to \pi\rho$.

	Our work	Experimental data
$\Gamma((\pi\rho)_S)/\Gamma_{Total}$	0.86	0.60 [3]
$\Gamma((\pi\rho)_D)/\Gamma_{Total}$	5.3×10^{-2}	$(1.30\pm0.60\pm0.22)\times10^{-2}$ [3]
$\Gamma_{\pi\sigma}/\Gamma_{Total}$	8.2×10^{-2}	$(18.76\pm4.29\pm1.48)\times10^{-2}$ [3]
$\Gamma_{\sigma\pi}/\Gamma_{(\rho\pi)_S}$	0.09	0.06 ± 0.05 [1]

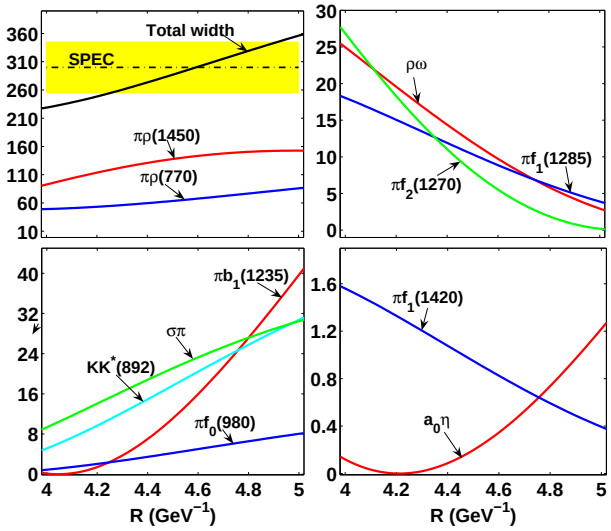

FIG. 3: (color online). R dependence of the decay behaviors of the $a_1(1640)$. Here, the dot-dashed line with band is the experimental total width in Ref. [5]. All results are in units of MeV.

considerable contributions to the total decay width. In Table VI, we also list some typical ratios relevant to their decays. We still need to emphasize one point. At present, $a_1(1930)$ and $a_1(2095)$ are not well established in experiment. The authors of Ref. [7] indicated that $a_2(1950)$ *and* $a_1(1930)$ *are not securely identified in mass and width, though some such contributions are definitely required* [7]. However, If considering the Regge trajectory analysis, one finds that a 3^3P_1 state in the a_1 meson family has the mass around 2000 MeV. Two unconfirmed $a_1(1930)$ and $a_1(2095)$ can be as the candidate of 3^3P_1 state in the a_1 meson family, since their masses are close to that of 3^3P_1 state in the a_1 meson family. Thus, experimental study of the partial decay widths of $a_1(1930)$ and $a_1(2095)$ will helpful to pin down two possible candidates, $a_1(1930)$ and $a_1(2095)$, of the second radial excitation of the $a_1(1260)$ to one. In the following, experimental confirmation of $a_1(1930)$ and $a_1(2095)$ will be crucial for identifying the candidate of a 3^3P_1 state in the a_1 meson family. If $a_1(1930)$ and $a_1(2095)$ cannot be established in experiment, we suggest experimental search for $a_1(3^3P_1)$, where the present results of $a_1(3^3P_1)$ predicted in this work are helpful to further exploration of it.

TABLE V: Typical ratios of the decay widths of the $a_1(1640)$ corresponding to the R range $(4.30 \sim 4.64)$ GeV^{-1}.

Ratio	Value	Ratio	Value
$\Gamma_{\pi\rho}/\Gamma_{Total}$	$0.216 \sim 0.227$	$\Gamma_{\pi\rho(1450)}/\Gamma_{Total}$	$0.473 \sim 0.474$
$\Gamma_{\pi b_1(1235)}/\Gamma_{Total}$	$0.014 \sim 0.059$	$\Gamma_{KK^*}/\Gamma_{\sigma\pi}$	$0.166 \sim 0.221$
$\Gamma_{\pi f_2(1270)}/\Gamma_{\rho\omega}$	$0.523 \sim 0.855$	$\Gamma_{\pi f_1(1420)}/\Gamma_{\pi f_1(1285)}$	$0.089 \sim 0.094$
$\Gamma_{\pi f_0}$	$0.166 \sim 0.221$		

TABLE VI: Typical ratios for the $a_1(1930)$ and $a_1(2095)$. The R ranges are $(4.58 \sim 4.92)$ GeV^{-1} and $(4.78 \sim 5.16)$ GeV^{-1} for the $a_1(1930)$ and $a_1(2095)$, respectively.

Ratio	$a_1(1930)$	$a_1(2095)$
$\Gamma_{\pi\rho}/\Gamma_{Total}$	$0.151 \sim 0.162$	$0.139 \sim 0.176$
$\Gamma_{\pi b_1(1235)}/\Gamma_{Total}$	$0.092 \sim 0.160$	$0.206 \sim 0.2542$
$\Gamma_{\pi\rho(1700)}/\Gamma_{Total}$	$0.005 \sim 0.024$	$0.039 \sim 0.0529$
$\Gamma_{\sigma\pi}/\Gamma_{Total}$	$0.088 \sim 0.097$	$0.058 \sim 0.073$
$\Gamma_{\pi\rho(1450)}/\Gamma_{Total}$	$0.339 \sim 0.347$	$0.189 \sim 0.253$
$\Gamma_{\pi b_1(1235)}/\Gamma_{\pi\rho(1450)}$	$0.271 \sim 0.462$	$0.348 \sim 1.813$
$\Gamma_{\eta a_1(1260)}/\Gamma_{KK^*(892)}$	$0.629 \sim 0.719$	$1.141 \sim 1.742$
$\Gamma_{\rho\omega}\Gamma_{\pi f_2(1270)}$	$0.705 \sim 0.850$	$0.188 \sim 0.451$
$\Gamma_{\eta a_0(980)}/\Gamma_{\pi\rho(1700)}$	$0.317 \sim 0.809$	$0.239 \sim 0.279$
$\Gamma_{KK_1(1400)}/\Gamma_{\eta a_2(1320)}$	$0.508 \sim 0.553$	$1.693 \sim 4.846$
$\Gamma_{KK_1(1400)}/\Gamma_{\rho a_0(980)}$	–	$0.145 \sim 0.184$
$\Gamma_{\eta a_0(1450)}/\Gamma_{KK_0^*(1430)}$	–	$0.206 \sim 0.838$

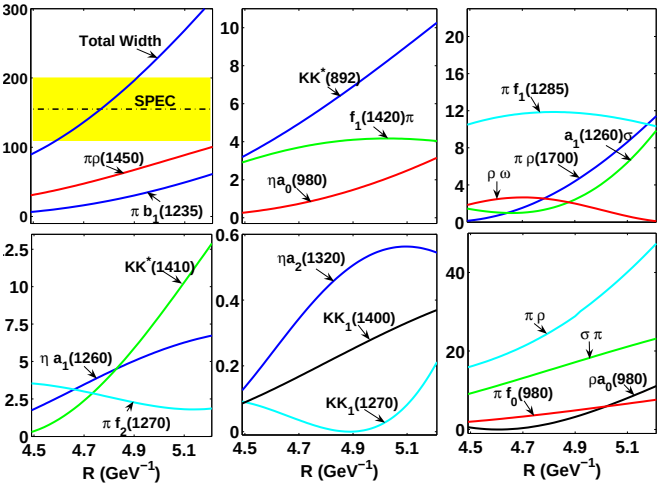

FIG. 4: (color online). R dependence of the calculated partial and total decay widths of the $a_1(1930)$. Here, the dot-dashed line with band is the experimental total width in Ref. [7]. All results are in units of MeV.

In Fig. 6, we discuss the decay behavior of the $a_1(2270)$ as the third radial excitation of the $a_1(1260)$. We find that the main decay mode includes decay channels, $\pi b_1(1235)$, $\pi\rho$, $\pi\rho(1450)$, and $\pi\rho(1700)$. In addition, $KK^*(1410)$, $\rho h_1(1170)$, $KK^*(1680)$, $\pi\sigma$, and $\sigma a_1(1260)$ have important contributions to the total decay width. The $\rho a_2(1320)$, $\eta'(958)a_0(980)$, and $K^*K_1(1270)$ are subordinate decay modes, which are not shown in Fig. 6. In Table VII, we also list the typical ratios of decays of the $a_1(2270)$.

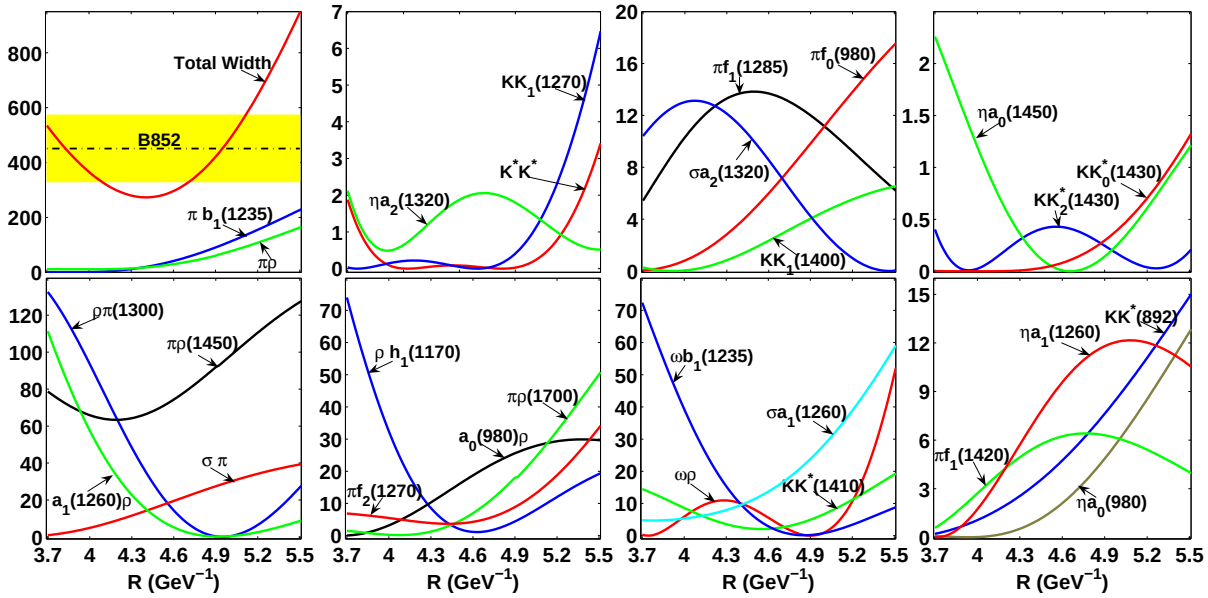

FIG. 5: (color online). R dependence of the calculated partial and total decay widths of the $a_1(2095)$. Here, the dot-dashed line with band is the experimental total width in Ref. [7]. All results are in units of MeV.

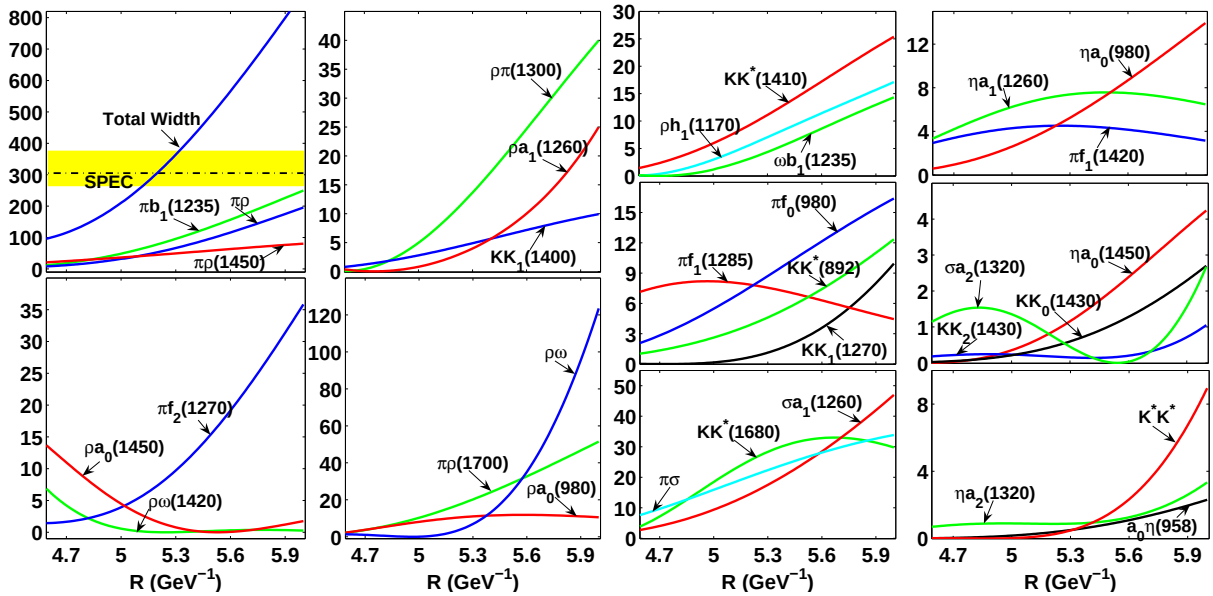

FIG. 6: (color online). R dependence of the calculated partial and total decay widths of the $a_1(2270)$. Here, the dot-dashed line with band is the experimental total width in Ref. [7]. All results are in units of MeV.

B. b_1 states

The Regge trajectory analysis indicates that the $b_1(1235)$, $b_1(1960)$, and $b_1(2240)$ are the ground state, the second radial excitation, and the third radial excitation in the b_1 meson family, respectively. In addition, we also predict a missing $b_1(1640)$ as the first radial excitation. In the following, we study their decays.

As for the $b_1(1235)$, there are two allowed decay channels, $\pi\omega$ and $\pi a_0(980)$. The result shown in Fig. 7 shows that the obtained total width overlaps with experimental data in Ref. [63]. Since $b_1 \to \omega\pi$ occurs via S and D waves, we obtain the D-wave/S-wave amplitude ratio of $b_1 \to \omega\pi$ process, which is 0.465 in our work which is consistent with the Crystal Barrel data (0.45 ± 0.04) [10]. On the other hand, the decay channel πf_0 has a partial decay width less than 1 MeV.

As a predicted b_1 state, $b_1(1640)$ has the decay behavior listed in Fig. 8, where we take the same R range as that

TABLE VII: Calculated ratios of decays of the $a_1(2270)$. Here, all the results correspond to the R range (5.12 ~ 5.32) GeV^{-1}.

Ratio	Value	Ratio	Value
$\Gamma_{\pi\rho}/\Gamma_{Total}$	0.164 ~ 0.184	$\Gamma_{\pi f_1(1285)}/\Gamma_{\pi\sigma}$	0.313 ~ 0.435
$\Gamma_{\pi b_1(1235)}/\Gamma_{Total}$	0.247 ~ 0.264	$\Gamma_{KK^*(892)}/\Gamma_{\eta a_1(1260)}$	0.313 ~ 0.487
$\Gamma_{\pi\rho_{1700}}/\Gamma_{Total}$	0.052 ~ 0.056	$\Gamma_{\pi f_1(1420)}/\Gamma_{\rho a_0(980)}$	0.404 ~ 0.469
$\Gamma_{\sigma\pi}/\Gamma_{Total}$	0.064 ~ 0.070	$\Gamma_{\eta a_0(980)}/\Gamma_{\pi f_2(1270)}$	0.532 ~ 0.612
$\Gamma_{\pi\rho(1450)}/\Gamma_{Total}$	0.134 ~ 0.157	$\Gamma_{\eta a_2(1320)}/\Gamma_{\pi f_0}$	0.099 ~ 0.131
$\Gamma_{\rho a_1(1260)}/\Gamma_{\omega b_1(1235)}$	0.789 ~ 0.926	$\Gamma_{\eta a_0(1450)}/\Gamma_{\omega b_1(1235)}$	0.236 ~ 0.273
$\Gamma_{KK_1(1400)}/\Gamma_{\rho\pi_{1300}}$	0.352 ~ 0.446	$\Gamma_{\eta a_1(1260)}/\Gamma_{KK^*(1680)}$	0.256 ~ 0.297
$\Gamma_{\rho h_1(1170)}/\Gamma_{KK_1(1400)}$	0.573 ~ 0.639	$\Gamma_{KK^*(1410)}/\Gamma_{\sigma a_1(1260)}$	0.633 ~ 0.638

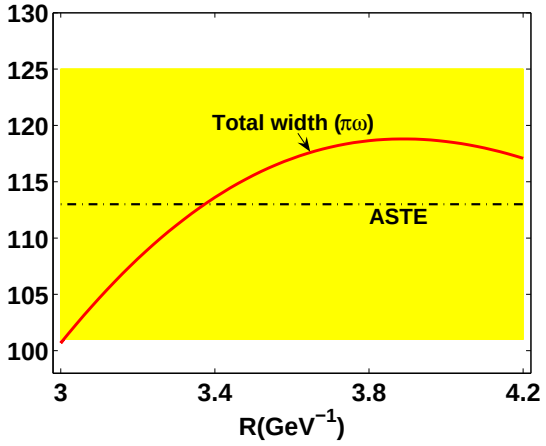

FIG. 7: (color online). R dependence of the calculated total decay width of the $b_1(1235)$. Here, the dot-dashed line with band is the experimental total width in Ref. [63]. The total decay width is in units of MeV.

for $a_1(1640)$[2]. Its main decay channel is $\pi a_0(980)$, while $\pi a_2(1320)$, $\rho\rho$, $\pi\omega(1420)$, KK^* and $\omega\pi$ also have considerable contributions to the total decay width. The total decay width is predicted to be 200 ~ 232 MeV. Table VIII shows some ratios relevant to the decays of $b_1(1640)$, which is valuable for further experimental search for this axial vector state.

[2] Since $b_1(1640)$ is as a predicted state, we take the same R range as that of $a_1(1640)$ to predict the decay behavior of $b_1(1640)$. This treatment is due to $b_1(1640)$ as the isospin partner of $a_1(1640)$, which have similar R range.

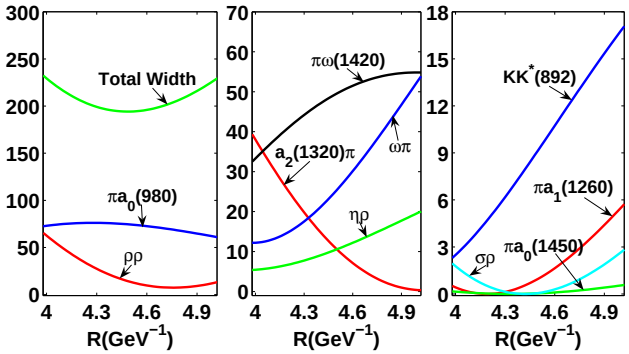

FIG. 8: (color online). R dependence of the calculated partial and total decay widths of the $b_1(1640)$. All results are in units of MeV.

TABLE VIII: Typical ratios for decays of the $b_1(1640)$ corresponding to R = 4.20 ~ 4.90 GeV^{-1}.

Ratio	Value	Ratio	Value
$\Gamma_{\pi a_0(980)}/\Gamma_{Total}$	0.352 ~ 0.368	$\Gamma_{KK^*}/\Gamma_{\omega\pi}$	0.324 ~ 0.347
$\Gamma_{\eta\rho}/\Gamma_{\pi\omega(1420)}$	0.164 ~ 0.263	$\Gamma_{\pi a_2(1320)}/\Gamma_{\rho\rho}$	0.565 ~ 0.681

Assuming the $b_1(1960)$ as the second radial excitation of the $b_1(1235)$, we present its total and partial decay widths in Fig. 9. Our calculated total width can cover the experimental data given in Ref. [12]. Its main decay channels are $\pi a_0(1450)$, $\pi\omega$, $\pi a_0(980)$ and $\pi\omega(1420)$, while the partial decay widths of the decay modes $\pi a_1(1260)$, $\rho\eta$, and $\pi a_2(1320)$ are also considerable. We also obtain some ratios of partial decay widths of the $b_1(1960)$ in Table IX.

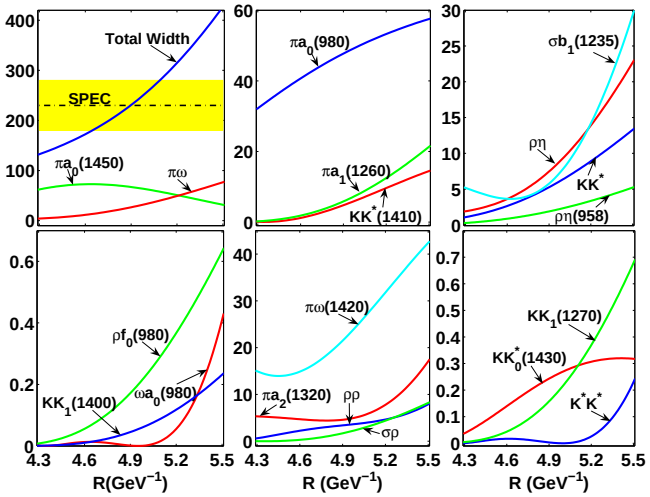

FIG. 9: (color online). R dependence of the calculated partial and total decay widths of the $b_1(1960)$. Here, the dot-dashed line with band is the experimental total width in Ref. [12]. Since the width of the KK_2^* mode is tiny, we do not list its contribution here. All results are in units of MeV.

In Fig. 10, We show the decay behavior of the $b_1(2240)$ as the third radial excitation of the $b_1(1235)$. Additionally, its main decay modes are $\omega\pi$, $\pi\omega(1420)$, $\pi a_0(980)$,

TABLE IX: Obtained ratios for decays of the $b_1(1960)$. All results correspond to $R = 4.66 \sim 5.16$ GeV^{-1}.

Ratio	Value	Ratio	Value
$\Gamma_{\pi a_0(980)}/\Gamma_{Total}$	$0.186 \sim 0.235$	$\Gamma_{\rho\rho}/\Gamma_{Total}$	$0.028 \sim 0.031$
$\Gamma_{\pi\omega_{1420}}/\Gamma_{Total}$	$0.088 \sim 0.107$	$\Gamma_{\omega\pi}/\Gamma_{Total}$	$0.077 \sim 0.162$
$\Gamma_{\rho\rho}/\Gamma_{\pi a_2(1320)}$	$0.572 \sim 0.624$	$\Gamma_{KK^*(892)}/\Gamma_{\eta\rho}$	$0.648 \sim 0.736$
$\Gamma_{\rho f_0}/\Gamma_{\pi a_1(1260)}$	$0.029 \sim 0.030$	$\Gamma_{KK_1(1400)}/\Gamma_{KK_1(1270)}$	$0.249 \sim 0.316$

$\pi a_0(1450)$. Of course, the decay modes $\rho\rho$, $\rho b_1(1235)$, $\pi a_2(1320)$, $\pi a_1(1260)$ also have obvious contributions to the total decay width. For convenience of further experimental study of this state, we provide information of typical ratios of the partial width of the $b_1(2240)$ in Table X.

TABLE X: Calculated ratio for the $b_1(2240)$ corresponding to $R = 5.20 \sim 5.54$ GeV^{-1}.

Ratio	Value	Ratio	Value
$\Gamma_{\pi a_0(980)}/\Gamma_{Total}$	$0.097 \sim 0.128$	$\Gamma_{\pi a_0(1450)}/\Gamma_{Total}$	$0.131 \sim 0.232$
$\Gamma_{\pi\omega_{1420}}/\Gamma_{Total}$	$0.068 \sim 0.071$	$\Gamma_{\omega\pi}/\Gamma_{Total}$	$0.179 \sim 0.199$
$\Gamma_{\pi a_2(1320)}/\Gamma_{Total}$	$0.075 \sim 0.102$	$\Gamma_{\pi a_1(1260)}$	$0.057 \sim 0.066$
$\Gamma_{\eta\rho(1450)}/\Gamma_{Total}$	$0.055 \sim 0.064$	$\Gamma_{\eta\rho}/\Gamma_{Total}$	$0.050 \sim 0.062$
$\Gamma_{KK^*(1680)}/\Gamma_{Total}$	$0.042 \sim 0.057$	$\Gamma_{\rho f_1(1285)}/\Gamma_{\omega a_1(1260)}$	$0.678 \sim 0.819$
$\Gamma_{\rho f_0}/\Gamma_{\rho b_1(1235)}$	$0.112 \sim 0.173$	$\Gamma_{\rho f_2(1270)}/\Gamma_{KK_1(1400)}$	$0.254 \sim 0.317$
$\Gamma_{KK_1(1270)}/\Gamma_{KK_0^*(1430)}$	$0.233 \sim 0.383$	$\Gamma_{\rho\eta'(958)}/\Gamma_{KK^*(1410)}$	$0.364 \sim 0.381$
$\Gamma_{KK^*(1410)}/\Gamma_{KK^*(892)}$	$0.903 \sim 0.950$	$\Gamma_{\omega a_0(980)}/\Gamma_{\omega a_1(1260)}$	$0.158 \sim 0.204$

C. f_1 states

When discussing f_1 states, we need to consider the admixtures of the flavor wave functions $|n\bar{n}\rangle = (|u\bar{u}\rangle + |d\bar{d}\rangle)/\sqrt{2}$ and $|s\bar{s}\rangle$. The $f_1(1285)$ and $f_1(1420)/f_1(1510)$ satisfy

$$\begin{pmatrix} |f_1(1285)\rangle \\ |f_1(1420)/f_1(1510)\rangle \end{pmatrix} = \begin{pmatrix} \cos\phi & -\sin\phi \\ \sin\phi & \cos\phi \end{pmatrix} \begin{pmatrix} |n\bar{n}\rangle \\ |s\bar{s}\rangle \end{pmatrix}, \quad (7)$$

where both the $f_1(1420)$ and $f_1(1510)$ are partners of the $f_1(1285)$. Later, we present their decay behaviors. ϕ denotes a mixing angel. This mixing angle was determined in a phenomenological way [64] and is given by $\phi = (20-30)^\circ$ which is consistent with $\phi = (24^{+3.2}_{-2.7})^\circ$ reported by the LHCb Collaboration [65] and $\phi = (21 \pm 5)^\circ$ from the updated Lattice QCD analysis [66]. When calculating the decays of the $f_1(1285)$ and $f_1(1420)/f_1(1510)$, we take the LHCb value $\phi = 24^\circ$.

In Fig. 1, we have predicted the $f_1(1640)$ as the first radial excitation of the $f_1(1285)$, while the $f_1(1800)$ as a partner of the $f_1(1640)$ is also predicted, where these two predicted axial vector mesons have relations

$$\begin{pmatrix} |f_1(1640)\rangle \\ |f_1(1800)\rangle \end{pmatrix} = \begin{pmatrix} \cos\phi_1 & -\sin\phi_1 \\ \sin\phi_1 & \cos\phi_1 \end{pmatrix} \begin{pmatrix} |n\bar{n}\rangle \\ |s\bar{s}\rangle \end{pmatrix}, \quad (8)$$

In addition, there exist relations among the $f_1(1970)$, the predicted $f_1(2110)$, $f_1(2210)$, and $f_1(2310)$, i.e.,

$$\begin{pmatrix} |f_1(1970)\rangle \\ |f_1(2110)\rangle \end{pmatrix} = \begin{pmatrix} \cos\phi_2 & -\sin\phi_2 \\ \sin\phi_2 & \cos\phi_2 \end{pmatrix} \begin{pmatrix} |n\bar{n}\rangle \\ |s\bar{s}\rangle \end{pmatrix}, \quad (9)$$

and

$$\begin{pmatrix} |f_1(2210)\rangle \\ |f_1(2310)\rangle \end{pmatrix} = \begin{pmatrix} \cos\phi_3 & -\sin\phi_3 \\ \sin\phi_3 & \cos\phi_3 \end{pmatrix} \begin{pmatrix} |n\bar{n}\rangle \\ |s\bar{s}\rangle \end{pmatrix}, \quad (10)$$

Here, the mixing angels ϕ_i $(i = 1, 2, 3)$ cannot be constrained by our analysis. In the following discussions, we take a typical value $\phi_i = \phi = 24^\circ$ to give the quantitative results.

As for the $f_1(1285)$, we show its partial and total decay widths in Fig. 11, where the calculated total decay width is in agreement with the experimental data in Ref. [67]. However, we notice that the calculated branching ratio for $\Gamma_{\pi a_0}/\Gamma_{total} = 0.67 \sim 0.68$ corresponding to $R = (3.00 \sim 4.00)$ GeV^{-1}, which is a little bit larger than $(36 \pm 7)\%$ listed in PDG [1]. The PDG data also shows that the branching ratio of its decay $\eta\pi\pi$ can reach up to $(52.4^{+1.9}_{-2.2})\%$ [1], which is the main contribution to the total decay width of the $f_1(1285)$. In this work, we study processes $f_1(1285) \to \eta\sigma \to \eta\pi\pi$ and $f_1(1285) \to \pi a_0(980) \to \eta\pi\pi$, which can be calculated by the QPC model. Thus, the decay width of $f_1(1285) \to \eta\sigma \to \eta\pi\pi$ can be written as [44]

$$\begin{aligned} &\Gamma(f_1 \to \eta + \sigma \to \eta + \pi\pi) \\ &= \frac{1}{\pi}\int_{4m_\pi^2}^{(m_{f_1}-m_\eta)^2} dr\,\sqrt{r}\frac{\Gamma_{f_1\to\eta+\sigma}(r)\cdot\Gamma_{\sigma\to\pi\pi}(r)}{(r-m_\sigma^2)^2+(m_\sigma\Gamma_\sigma)^2}, \end{aligned} \quad (11)$$

where the interaction of σ with two pions can be described by the effective Lagrangian

$$\mathcal{L}_{\sigma\pi\pi} = g_\sigma\sigma(2\pi^+\pi^- + \pi^0\pi^0). \quad (12)$$

The coupling constant $g_\sigma = 2.12 \sim 2.81$ GeV is determined by the total width $\Gamma_\sigma = 400 \sim 700$ MeV [1], and the decay width reads as

$$\Gamma_{\sigma\to\pi\pi}(r) = \frac{g_\sigma^2\lambda^2}{8\pi r}\frac{[(r-(2m_\pi)^2)r]^{1/2}}{2\sqrt{r}}, \quad (13)$$

where λ is $\sqrt{2}$ and 1 for $\pi^+\pi^-$ and $\pi^0\pi^0$, respectively.

The process $f_1(1285) \to \pi a_0(980) \to \eta\pi\pi$ is calculated in a similar way and the equation is given by

$$\begin{aligned} &\Gamma(f_1 \to a_0 + \pi \to \eta + \pi\pi) \\ &= \frac{1}{\pi}\int_{(m_\pi+m_\eta)^2}^{(m_{f_1}-m_\pi)^2} dr\,\sqrt{r}\frac{\Gamma_{f_1\to\pi+a_0}(r)\cdot\Gamma_{a_0\to\eta\pi}(r)}{(r-m_{a_0}^2)^2+(m_{a_0}\Gamma_{a_0})^2}, \end{aligned} \quad (14)$$

where the decay width for $a_0(980) \to \eta\pi$ is

$$\begin{aligned} &\Gamma_{a_0(980)\to\eta\pi}(r) \\ &= \frac{g_{a_0}^2}{8\pi r}\frac{[(r-(m_\eta+m_\pi)^2)(r-(m_\eta-m_\pi))^2]^{1/2}}{2\sqrt{r}}, \end{aligned} \quad (15)$$

where the coupling constant $g_{a_0} = 1.262 \sim 2.524$ GeV is determined by the total width of $a_0(980)$ ($\Gamma_{a_0(980)} =$

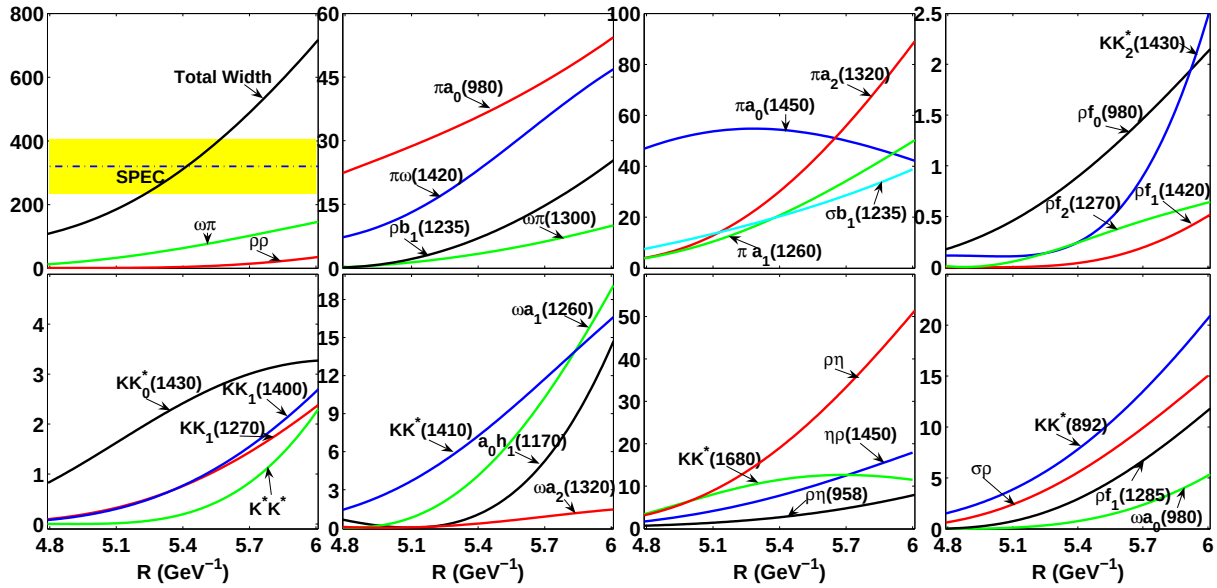

FIG. 10: (color online). R dependence of the calculated partial and total decay widths of the $b_1(2240)$. Here, the dot-dashed line with band is the experimental total width in Ref. [12]. We do not present the $K^*K_1(1270)$ contribution since this decay has tiny width. All results are in units of MeV.

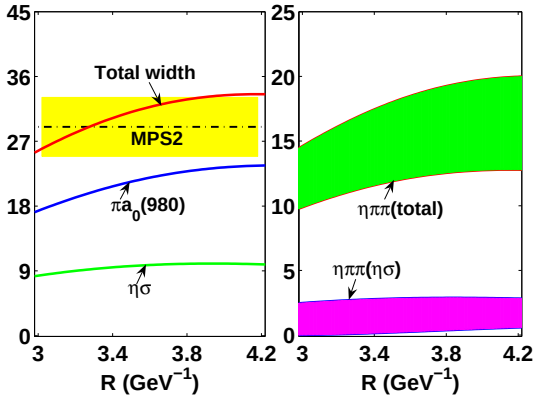

FIG. 11: (color online). R dependence of the total and partial decay widths of the $f_1(1285)$. We also present the decay width of $f_1(1285) \to \eta\pi\pi$ via the intermediate channels $\eta\sigma$ and $\pi a_0(980)$ (green band), and only from the intermediate channel $\eta\sigma$ (pink band). Here, the experimental total width from Ref. [67] is denoted by the dot-dashed line with band. All results are in units of MeV.

50 ∼ 100 MeV). The final result of the width of $f_1(1285) \to \pi a_0(980) \to \eta\pi\pi$ includes the contributions from both $\eta\pi^0\pi^0$ and $\eta\pi^+\pi^-$.

The decay width of $f_1(1285) \to \eta\pi\pi$ via the intermediate $\eta\sigma$ and $\pi a_0(980)$ channels, and only from the intermediate $\eta\sigma$ channel are shown in Fig. 11. In addition, the decay width of $f_1(1285) \to \eta\pi\pi$ from the intermediate $\pi a_0(980)$ channel is comparable with the corresponding experimental data ((16 ± 7)%) in PDG [1].

In the following, we discuss decay behaviors of the $f_1(1420)$ and $f_1(1510)$ as partners of the $f_1(1285)$. As for the $f_1(1420)$, the obtained total decay width can overlap with the DM2 result [68] as shown in Fig. 12. Its main decay channel is KK^*. Thus, the present study of decay of the $f_1(1420)$ supports the $f_1(1420)$ as a partner of the $f_1(1285)$. As for the $f_1(1510)$, its partial and total decay widths are listed in Fig .13, which shows that the calculated total decay width is larger than the experimental data [68]. Thus, the $f_1(1510)$ as a partner of the $f_1(1285)$ can be excluded.

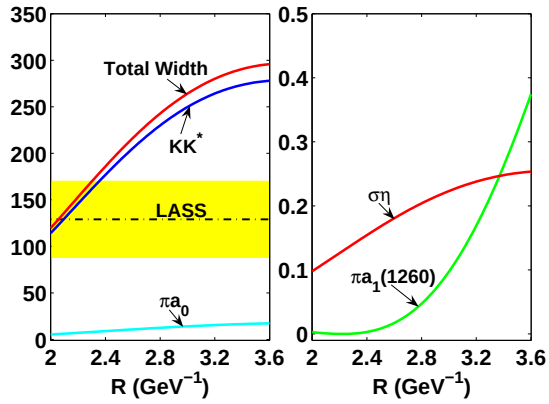

FIG. 12: (color online). R dependence of the total and partial decay widths of $f_1(1420)$. Here, the experimental total width in Ref. [68] is shown by the dot-dashed line with band. All results are in units of MeV.

In Figs. 14-15, we further illustrate the decay properties of two predicted states $f_1(1640)$ and $f_1(1800)$. In addition, we also list some of their typical ratios, which are weakly dependent on the R value (see Table XI), where we take $R = (3.60 \sim 4.40)$ GeV^{-1}. From Figs. 14-15 and Table XI, we can obtain information of the main decay modes and the

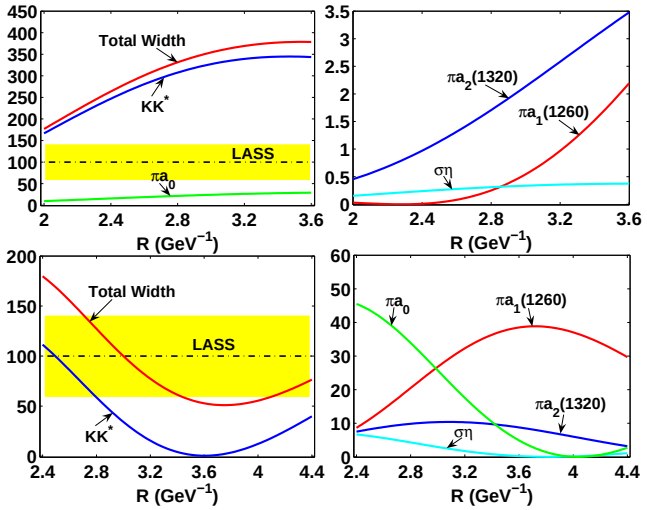

FIG. 13: (color online). Total and partial decay widths of the $f_1(1510)$ as a partner of the $f_1(1285)$ (the first row) and as the first radial excitation of the $f_1(1285)$ (the second row). The experimental total width in Ref. [69] is denoted by the dot-dashed line with band. All results are in units of MeV.

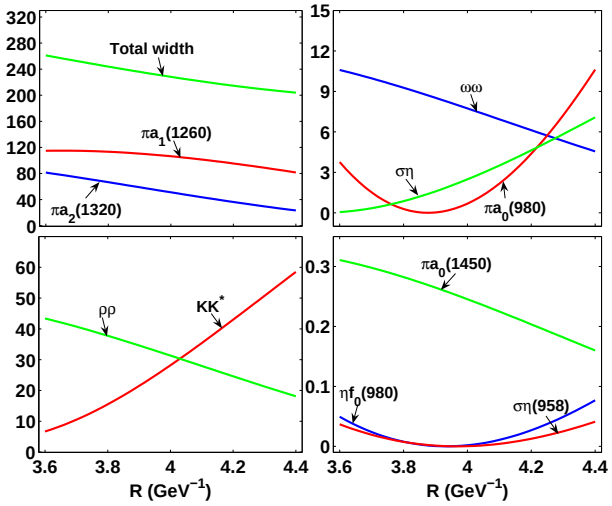

FIG. 14: (color online). R dependence of the total and partial decay widths of $f_1(1640)$. All results are in units of MeV.

TABLE XI: Some obtained ratios relevant to decays of the $f_1(1640)$ and $f_1(1800)$. All values correspond to the R range (3.60 ~ 4.40) GeV^{-1}.

$f_1(1640)$		$f_1(1800)$	
$\Gamma_{\pi a_1(1260)}/\Gamma_{Total}$	0.400 ~ 0.440	$\Gamma_{\rho\rho}/\Gamma_{Total}$	0.102 ~ 0.290
$\Gamma_{\pi a_2(1320)}/\Gamma_{Total}$	0.114 ~ 0.312	$\Gamma_{\omega\omega}/\Gamma_{\pi a_1(1260)}$	0.254 ~ 0.665
$\Gamma_{\omega\omega}/\Gamma_{\rho\rho}$	0.244 ~ 0.254	$\Gamma_{KK_1(1270)}/\Gamma_{KK^*}$	0.088 ~ 0.141
$\Gamma_{KK^*}/\Gamma_{Total}$	0.026 ~ 0.284	$\Gamma_{\pi a_2(1320)}/\Gamma_{Total}$	0.043 ~ 0.162

resonance parameters of two predicted f_1 mesons.

As for the $f_1(1510)$, there also exists another possible assignment, i.e., the $f_1(1510)$ can be as a radial excitation of the $f_1(1285)$ since the mass of $f_1(1510)$ is close to that of the predicted $f_1(1640)$. Here, we use the mixing angle expression

$$|f_1(1510)\rangle = \cos\phi_1|n\bar{n}\rangle - \sin\phi_1|s\bar{s}\rangle, \qquad (16)$$

which is the same as $f_1(1640)$. Thus, we also further illustrate the decay behavior of $f_1(1510)$ as a radial excitation of the $f_1(1285)$ (see Fig. 13). Under this assignment, the obtained total decay width can be fitted with the LASS data [69]. The KK^* mode also has a large contribution to the total decay width. These facts indicate that the $f_1(1510)$ as a radial excitation of the $f_1(1285)$ is possible.

In Fig. 16, we show the R dependence of decay behavior of the $f_1(1970)$ as the second radial excitation of the $f_1(1285)$. Its main decay channels are $KK^*(1410)$, $\pi a_0(980)$, $\pi a_1(1260)$, and KK^*. As a partner of the $f_1(1970)$, the predicted $f_1(2110)$ mainly decays into $KK_1(1270)$, $KK^*(1410)$, and KK^* and has a large total decay width as shown in Fig. 17.

The third radial excitation of the $f_1(1285)$ is still missing in experiment. In this work, we predict the $f_1(2210)$, for which its total and partial decay widths are calculated (see Fig. 18).

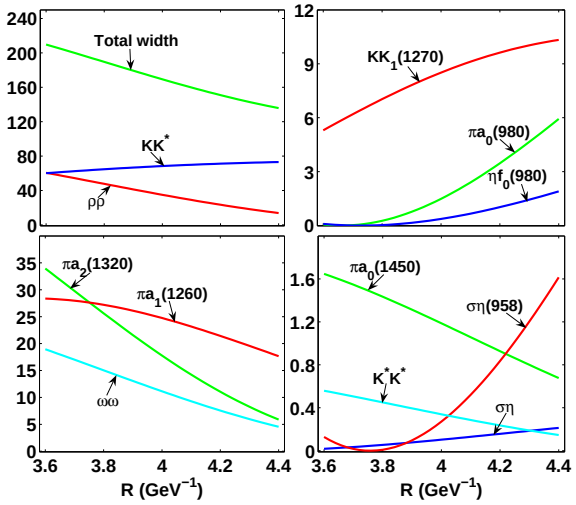

FIG. 15: (color online). R dependence of the total and partial decay widths of $f_1(1800)$. All results are in units of MeV.

As a partner of this predicted $f_1(2210)$, the $f_1(2310)$ has the decay properties listed in Fig. 19, in which the experimental width [24] is depicted by our calculation when taking R = (4.58 ~ 5.10) GeV^{-1}. Its main decay channels are $KK_1(1270)$, $KK^*(1680)$, $KK^*(1410)$, and KK^*.

D. h_1 states

Similar to the f_1 mesons, the following study of h_1 states is relevant to the admixtures of flavor wave functions $n\bar{n}$ and $s\bar{s}$. As the ground states in the h_1 meson family, the $h_1(1170)$ and

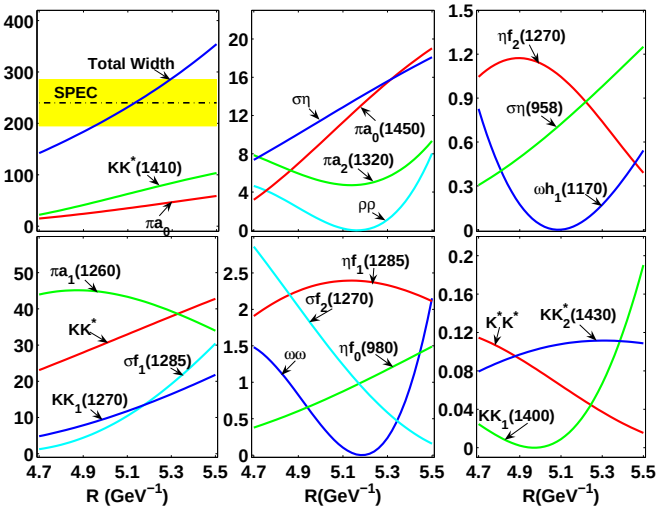

FIG. 16: (color online). R dependence of the total and partial decay widths of the $f_1(1970)$. The experimental total width from Ref. [24] is denoted by the dot-dashed line with band. All results are in units of MeV.

$h_1(1380)$ satisfy

$$\begin{pmatrix} |h_1(1170)\rangle \\ -|h_1(1380)\rangle \end{pmatrix} = \begin{pmatrix} \sin\theta_1 & \cos\theta_1 \\ -\cos\theta_1 & \sin\theta_1 \end{pmatrix} \begin{pmatrix} |n\bar{n}\rangle \\ |s\bar{s}\rangle \end{pmatrix}, \tag{17}$$

where the mixing angle θ_1 is introduced, the first line of this equation is adopted in this paper, and the second line is used in Ref. [70]. In Ref. [70], Cheng obtained $\theta_1 \sim 82.7^\circ$. The calculation of Lattice QCD indicates $\theta_1 = 86.8^\circ$ [71]. In addition, $\theta_1 = 85.6^\circ$ was obtained in Ref. [72]. In our calculation, we present our result as $\theta_1 = 85.6^\circ$.

The obtained partial and total decay widths of the $h_1(1170)$ and $h_1(1380)$ are shown in Fig. 20. Our results indicate that the $h_1(1170)$ and $h_1(1380)$ as the ground states in the h_1 meson family is suitable. Our result that the $h_1(1380)$ mainly decays into KK^* is consistent with the experimental fact that the $h_1(1380)$ has a dominant $s\bar{s}$ component [21, 28].

According to the Regge trajectory analysis in Fig. 1, the $h_1(1595)$, $h_1(1965)$, and $h_1(2215)$ are the first, the second and the third radial excitations of $h_1(1170)$. Here, the $h_1(1595)$, $h_1(1965)$, and $h_1(2215)$ have the same flavor wave functions as that of the $h_1(1170)$ in Eq. (17). The mixing angel θ_1 in Eq. (17) is replaced by θ_2, θ_3, and θ_4 for the corresponding h_1 states. As for these higher radial excitations, the mixing angels θ_i $(i = 2, 3, 4)$ were not well determined. Thus, we take a typical mixing angel $\theta_i = 85.6^\circ$ to discuss the decay behaviors of $h_1(1595)$, $h_1(1965)$, and $h_1(2215)$.

As for the $h_1(1595)$, we find that the obtained total decay width is much smaller than $384 \pm 60^{+70}_{-100}$ MeV measured by the BNL-E852 Collaboration [29]. Thus, we suggest to do the precise measurement of resonance parameters of the $h_1(1595)$, which is helpful to clarify this discrepancy. The result shown in Fig. 21 indicates that $\pi\rho$ is a dominant decay mode of the $h_1(1595)$. In addition, $h_1(1595) \to \omega\eta$ has a sizable contribution to the total decay width, which explains why the $\omega\eta$ mode was found in Ref. [73]. As the predicted partner of $h_1(1595)$, the $h_1(1780)$ dominantly decays into KK^* as presented in Fig. 21.

Figure 22 presents the results of the $h_1(1965)$, where the calculated total decay width can overlap with the Crystal Barrel data [30] when $R = (5.02 \sim 5.28)$ GeV^{-1}. Its main decay channels are $\pi\rho$, $\pi\rho(1450)$, and $\pi\rho(1700)$, while $\sigma h_1(1170)$ also provides a considerable value. As a partner of $h_1(1965)$, the $h_1(2120)$ is predicted in this work, where its main decay modes are KK^*, $KK^*(1410)$, and $KK_0^*(1430)$ (see Fig. 23 for more details of its decay properties).

The total and partial decay widths of the $h_1(2215)$ and its partner $h_1(2340)$ predicted in this work are listed in Figs. 24 and 25, respectively. The main decay modes of the $h_1(2215)$ and $h_1(2340)$ can be found in Figures 24 and 25.

III. DISCUSSION AND CONCLUSION

Although there are abundant axial vector states in PDG [1], the properties of the observed axial vector states are still unclear till now. The present unsatisfactory research status of the observed axial vector states stimulates us to systematically study them, which will be helpful for revealing their underlying structures. As a crucial step, we have studied whether the observed axial vector states can be categorized into the axial vector meson family.

In this work, we have discussed the observed axial vector states by assigning them as conventional states in the axial vector meson family, where both analysis of the mass spectra and calculation of their two-body OZI-allowed strong decays have been performed.

In our calculation via the QPC model, we take different R range for reproducing the total width of discussed axial vector states. With the discussed a_1 and b_1 states as an example, we listed the obtained R values for different states (see Table XII for more details). We find that the corresponding R values become more and more larger with increasing the radial quantum number, which is consistent with our understanding, i.e., the size of higher radial excitation is larger than that of lower radial excitation. Thus, our calculation can reflect this phenomenon, which provide a test of the reliability of our calculation. In addition, we also notice that the states with the same radial quantum number in the a_1 and b_1 families have similar R range, which reflects the fact that the a_1 state is as the isospin partner of the corresponding b_1 state.

When we discuss the decay behaviors of higher radial excitations in the f_1 and h_1 meson families, we fix the corresponding mixing angle to present the numerical results, which is due to the absence of theoretical study of these mixing angles. And these mixing angles cannot be determined by the present experimental data [1]. However, for the ground states of f_1 and h_1, the situation is totally different, where the corresponding mixing angles are fixed by experimental data. Thus, in this work we adopt a very simple and crude approach, i.e., we take the same value of mixing angle for ground and the corresponding radial excitations. We expect more experimen-

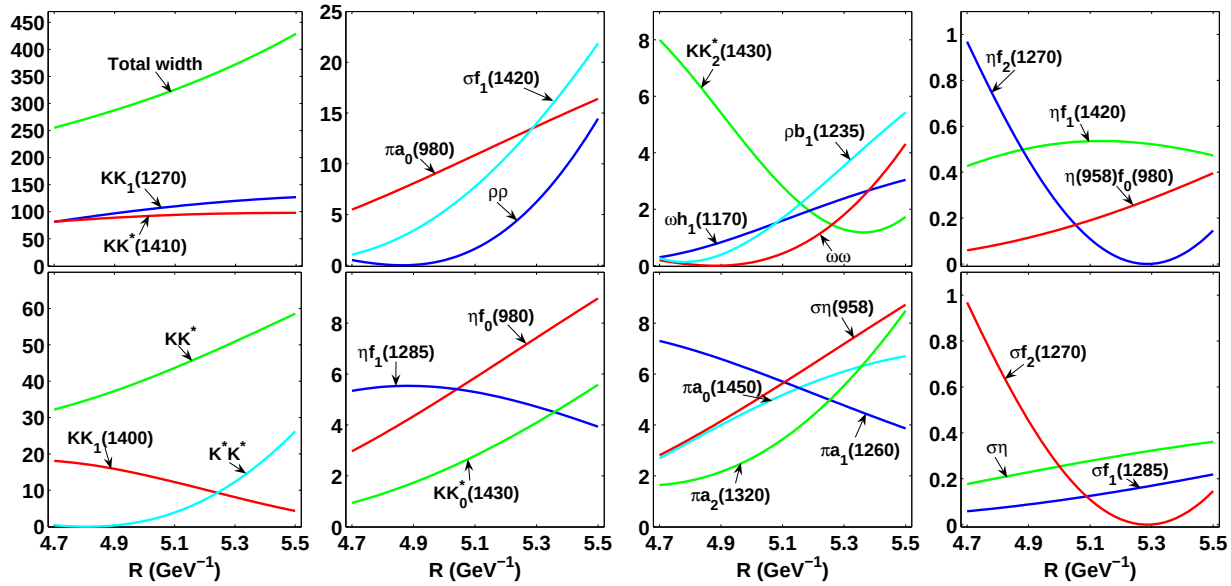

FIG. 17: (color online). R dependence of the total and partial decay widths of the $f_1(2110)$. All results are in units of MeV.

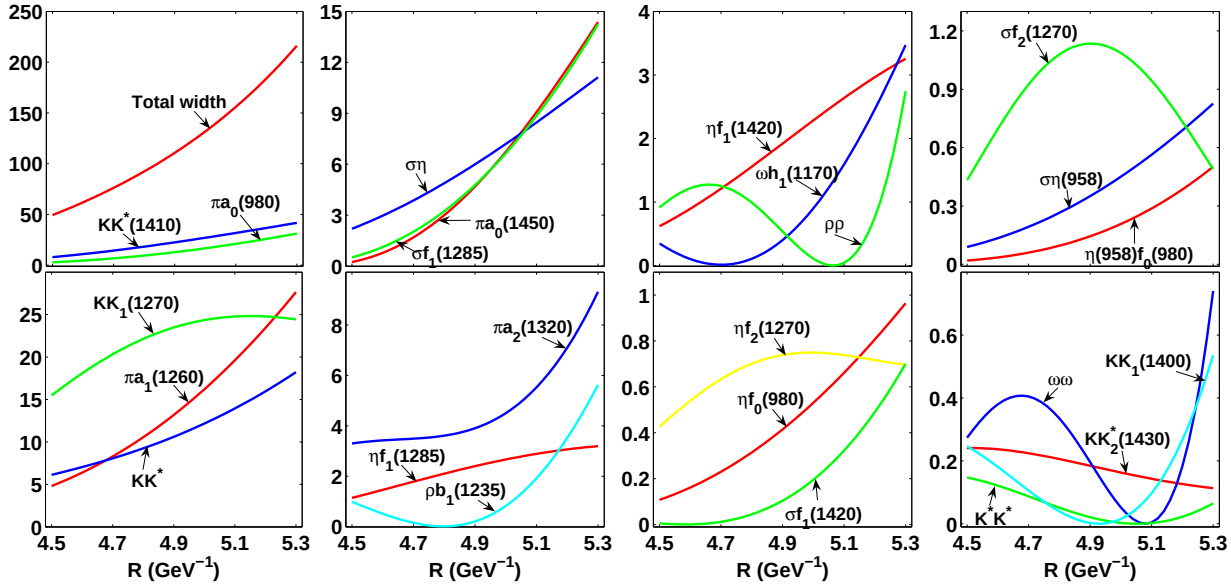

FIG. 18: (color online). R dependence of the total and partial decay widths of the $f_1(2210)$ on R value. All results are in units of MeV.

tal data of radial excitations in the f_1 and h_1 meson families. Then we can carry out further theoretical study by considering the effect of the mixing angle.

In summary, this phenomenological analysis not only tests possible assignments of the axial vector states, but also predicts abundant information of their partial decays, which is valuable for further experimental study of the observed states. In addition, we have also predicted some missing axial vector mesons, where their rough mass values and decay behaviors have been given. We have also suggested an experimental search for the missing states, where the BESIII and COMPASS experiments will be a good platform to carry out the study of light hadron spectra.

Acknowledgments

This project is supported by the National Science Foundation for Fostering Talents in Basic Research of the National Natural Science Foundation of China and the National Natural Science Foundation of China under Grants No. 11222547 and No. 11175073, the Ministry of Education of China (SRFDP under Grant No. 2012021111000), and the Fok Ying Tung Education Foundation (Grant No. 131006).

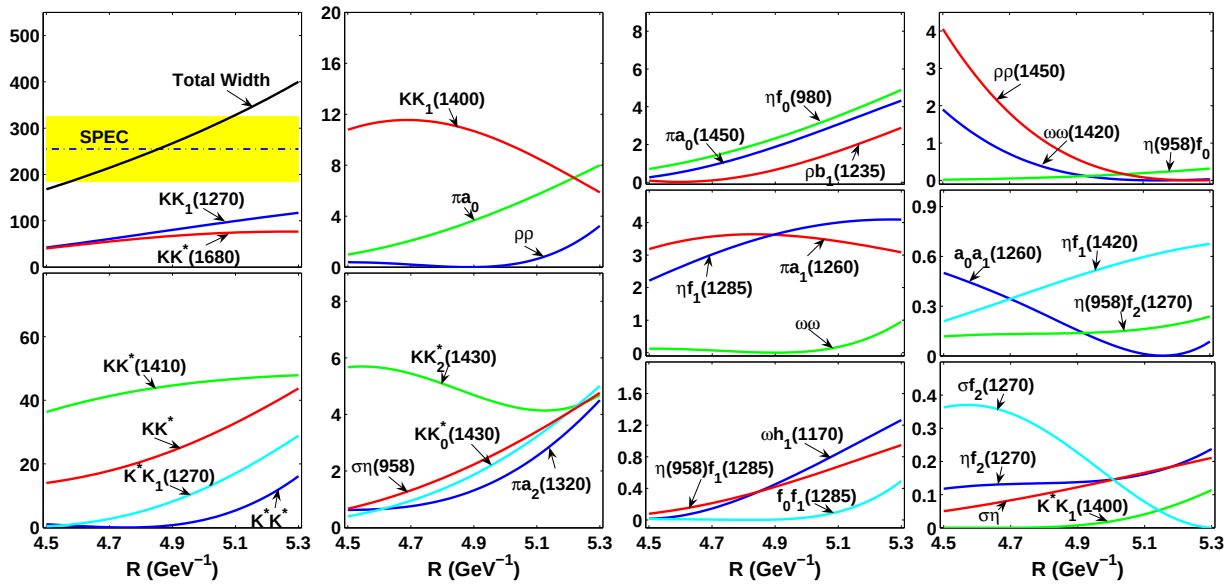

FIG. 19: (color online). R dependence of the total and partial decay widths of $f_1(2310)$. The experimental total width in Ref. [24] is denoted by the dot-dashed line with band. All results are in units of MeV.

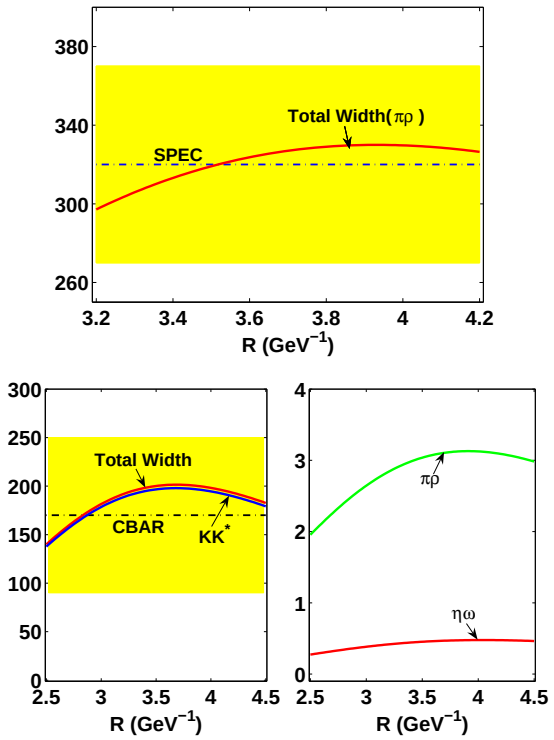

FIG. 20: (color online). R dependence of the total decay width of the $h_1(1170)$ (up) and the $h_1(1380)$ (down). Here, the dot-dashed lines with band are from Refs. [25, 28]. All results are in units of MeV.

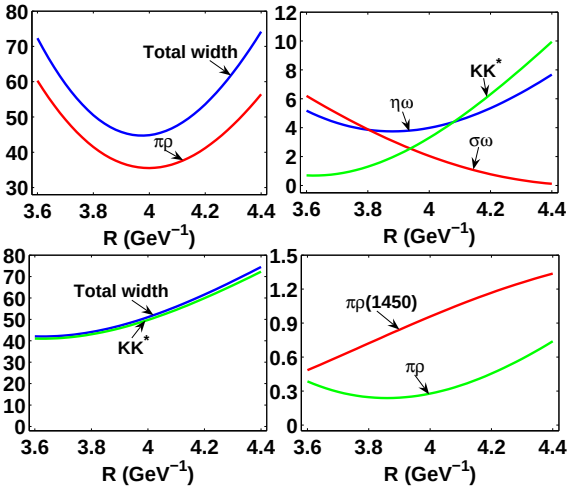

FIG. 21: (color online). R dependence of the total and partial decay widths of the $h_1(1595)$ (up) and the $h_1(1780)$ (down). All results are in units of MeV.

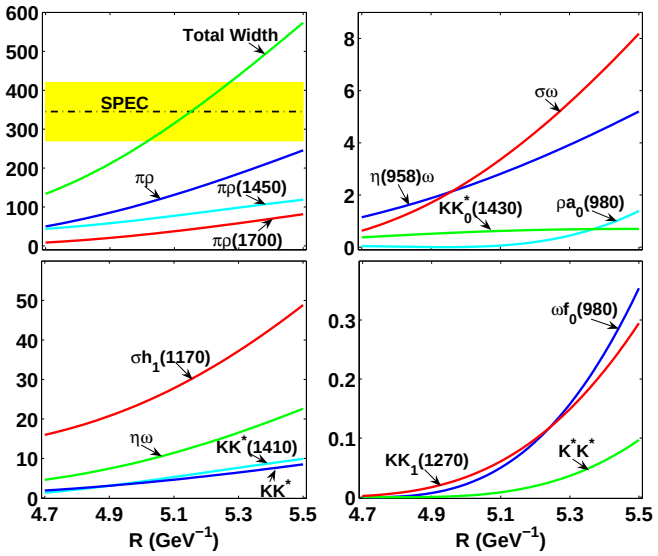

FIG. 22: (color online). R dependence of the total and partial decay widths of the $h_1(1965)$. The experimental total width from Ref. [30] is denoted by the dot-dashed line with band. All results are in units of MeV.

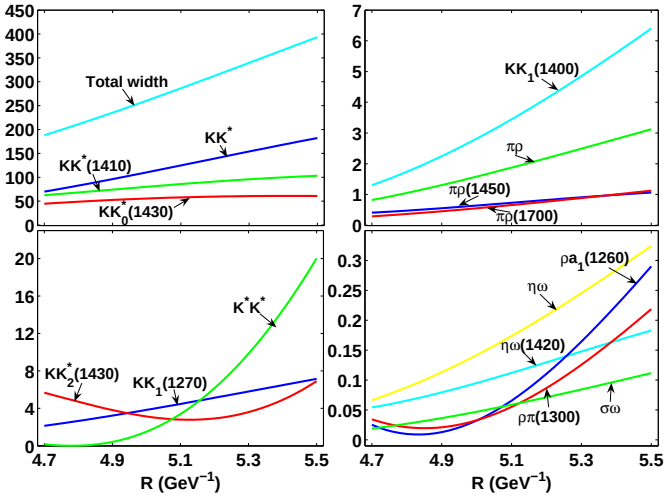

FIG. 23: (color online). R dependence of the total and partial decay widths of $h_1(2120)$. All results are in units of MeV.

TABLE XII: The obtained R value for these discussed a_1 and b_1 states in this work.

state	$n^{2S+1}L_J$	R (GeV^{-1})	state	$n^{2S+1}L_J$	R (GeV^{-1})
$a_1(1260)$	1^3P_1	3.846	$b_1(1235)$	1^1P_1	3.704
$a_1(1640)$	2^3P_1	4.30 ~ 4.64	$b_1(1640)$	2^1P_1	
$a_1(1930)$	3^3P_1	4.58 ~ 4.92	$b_1(1960)$	3^1P_1	4.66 ~ 5.16
$a_1(2095)$	3^3P_1	4.78 ~ 5.16			
$a_1(2270)$	4^3P_1	5.12 ~ 5.32	$b_1(2240)$	4^1P_1	5.20 ~ 5.54

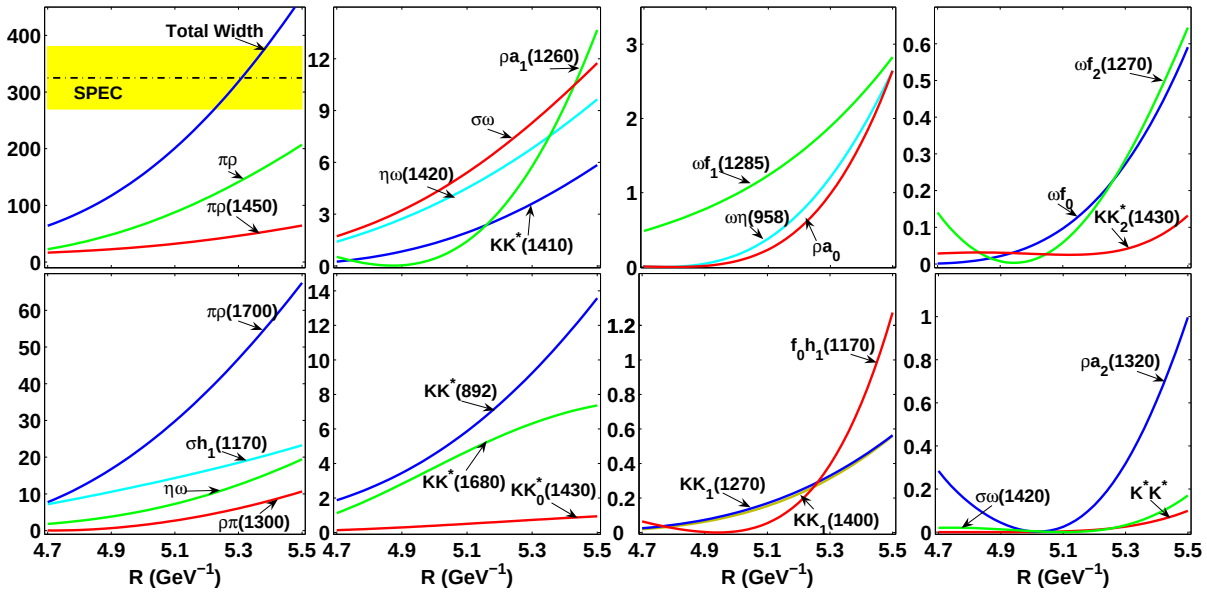

FIG. 24: (color online). R dependence of the total decay width of the $h_1(2215)$. The experimental total width in Ref. [30] is denoted by the dot-dashed line with band. All results are in units of MeV.

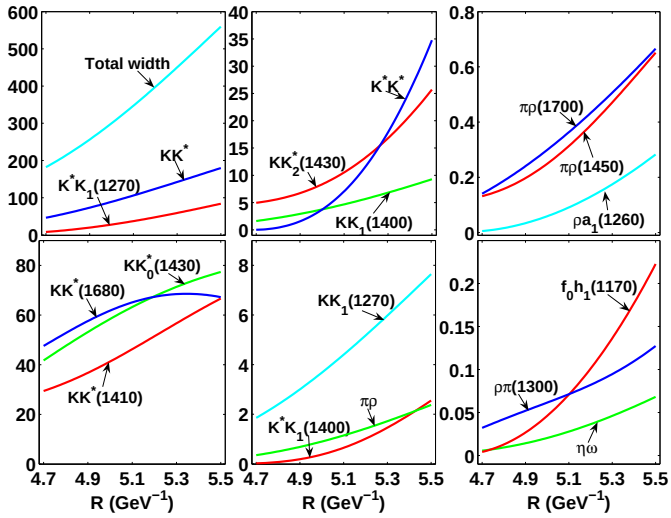

FIG. 25: (color online). R dependence of the total decay width of the $h_1(2340)$. All results are in units of MeV.

[1] K. A. Olive *et al.* [Particle Data Group Collaboration], Chin. Revs. C **38**, 090001 (2014).

[2] D. Barberis *et al.* [WA102 Collaboration], Phys. Lett. B **507**, 14 (2001) [hep-ex/0104017].

[3] D. M. Asner *et al.* [CLEO Collaboration], Phys. Rev. D **61**, 012002 (2000) [hep-ex/9902022].

[4] S. U. Chung, K. Danyo, R. W. Hackenburg, C. Olchanski, J. S. Suh, H. J. Willutzki, S. P. Denisov and V. Dorofeev *et al.*, Phys. Rev. D **65**, 072001 (2002).

[5] C. A. Baker, C. J. Batty, C. N. Pinder, P. Blum, C. Holtzhaussen, D. V. Bugg, C. Hodd and D. Odoom *et al.*, Phys. Lett. B **449**, 114 (1999).

[6] D. V. Amelin *et al.* [VES Collaboration], Phys. Lett. B **356**, 595 (1995).

[7] A. V. Anisovich, C. A. Baker, C. J. Batty, D. V. Bugg, V. A. Nikonov, A. V. Sarantsev, V. V. Sarantsev and B. S. Zou, Phys. Lett. B **517**, 261 (2001) [arXiv:1110.0278 [hep-ex]].

[8] J. Kuhn *et al.* [E852 Collaboration], Phys. Lett. B **595**, 109 (2004) [hep-ex/0401004].

[9] U. Karshon, G. Mikenberg, Y. Eisenberg, S. Pitluck, E. E. Ronat, A. Shapira and G. Yekutieli, Phys. Rev. D **10**, 3608 (1974).

[10] C. Amsler *et al.* [Crystal Barrel Collaboration], Phys. Lett. B **311**, 362 (1993).

[11] M. Nozar *et al.* [E852 Collaboration], Phys. Lett. B **541**, 35 (2002) [hep-ex/0206026].

[12] A. V. Anisovich, C. A. Baker, C. J. Batty, D. V. Bugg, L. Montanet, V. A. Nikonov, A. V. Sarantsev and V. V. Sarantsev *et al.*, Phys. Lett. B **542**, 8 (2002) [arXiv:1109.5247 [hep-ex]].

[13] D. Barberis *et al.* [WA102 Collaboration], Phys. Lett. B **471**, 440 (2000) [hep-ex/9912005].

[14] V. Dorofeev, A. Ekimov, Y. Gouz, A. Ivashin, I. Kachaev, A. Karyukhin, Y. Khokhlov and V. Konstantinov *et al.*, Eur. Phys. J. A **47**, 68 (2011).

[15] M. J. Corden, J. D. Dowell, J. Garvey, M. Jobes, I. R. Kenyon, J. Mawson, T. J. McMahon and I. F. Corbett *et al.*, Nucl. Phys. B **144**, 253 (1978).

[16] A. Gurtu *et al.* [Amsterdam-CERN-Nijmegen-Oxford Collaboration], Nucl. Phys. B **151**, 181 (1979).

[17] T. Bolton, J. S. Brown, K. Bunnell, M. Burchell, T. Burnett, R. Cassell, D. Coffman and D. H. Coward *et al.*, Phys. Lett. B **278**, 495 (1992).

[18] D. Barberis *et al.* [WA102 Collaboration], Phys. Lett. B **440**, 225 (1998) [hep-ex/9810003].

[19] C. Bromberg, J. Dickey, G. Fox, R. Gomez, W. Kropac, J. Pine, S. Stampke and H. Haggerty *et al.*, Phys. Rev. D **22**, 1513 (1980).

[20] C. Dionisi *et al.* [CERN-College de France-Madrid-Stockholm Collaboration], Nucl. Phys. B **169**, 1 (1980).

[21] D. Aston, N. Awaji, T. Bienz, F. Bird, J. D'Amore, W. M. Dunwoodie, R. Endorf and K. Fujii *et al.*, Phys. Lett. B **201**, 573 (1988).

[22] A. Birman, S. U. Chung, D. Peaslee, R. C. Fernow, H. Kirk, S. D. Protopopescu, D. Weygand and H. J. Willutzki *et al.*, Phys. Rev. Lett. **61**, 1557 (1988) [Erratum-ibid. **62**, 1577 (1989)].

[23] M. Ablikim *et al.* [BESIII Collaboration], Phys. Rev. Lett. **106**, 072002 (2011) [arXiv:1012.3510 [hep-ex]].

[24] A. V. Anisovich, C. A. Baker, C. J. Batty, D. V. Bugg, C. Hodd, H. C. Lu, V. A. Nikonov and A. V. Sarantsev *et al.*, Phys. Lett. B **491**, 47 (2000) [arXiv:1109.0883 [hep-ex]].

[25] J. A. Dankowych, P. Brockman, K. W. Edwards, J. Gandsman, D. Legacey, R. S. Longacre, J. F. Martin and P. M. Patel *et al.*, Phys. Rev. Lett. **46**, 580 (1981).

[26] M. Atkinson *et al.* [Omega Photon and Bonn-CERN-Glasgow-Lancaster-Manchester-Paris-Rutherford-Sheffield Collaborations], Nucl. Phys. B **231**, 15 (1984).

[27] A. Ando, K. Imai, S. Inaba, T. Inagaki, Y. Inagaki, A. Itano, S. Kobayashi and K. Maruyama *et al.*, Phys. Lett. B **291**, 496 (1992).

[28] A. Abele *et al.* [Crystal Barrel Collaboration], Phys. Lett. B **415**, 280 (1997).

[29] P. Eugenio *et al.* [BNL-E852 Collaboration], Phys. Lett. B **497**, 190 (2001) [hep-ph/0010337].

[30] A. V. Anisovich, C. A. Baker, C. J. Batty, D. V. Bugg, L. Montanet, V. A. Nikonov, A. V. Sarantsev and V. V. Sarantsev *et al.*, Phys. Lett. B **542**, 19 (2002) [arXiv:1109.5817 [hep-ex]].

[31] A. V. Anisovich, V. V. Anisovich and A. V. Sarantsev, Phys. Rev. D **62**, 051502 (2000) [hep-ph/0003113].

[32] L. Micu, Nucl. Phys. B **10**, 521 (1969).

[33] A. Le Yaouanc, L. Oliver, O. Pene and J. C. Raynal, Phys. Lett. B **72**, 57 (1977).

[34] A. Le Yaouanc, L. Oliver, O. Pene and J. -C. Raynal, Phys. Lett. B **71**, 397 (1977).

[35] A. Le Yaouanc, L. Oliver, O. Pene and J. C. Raynal, Phys. Rev. D **11**, 1272 (1975).

[36] A. Le Yaouanc, L. Oliver, O. Pene and J. -C. Raynal, Phys. Rev. D **9**, 1415 (1974).

[37] A. Le Yaouanc, L. Oliver, O. Pene and J. C. Raynal, Phys. Rev. D **8**, 2223 (1973).

[38] E. S. Ackleh, T. Barnes and E. S. Swanson, Phys. Rev. D **54**, 6811 (1996) [hep-ph/9604355].

[39] H. G. Blundell, hep-ph/9608473.

[40] R. Bonnaz, B. Silvestre-Brac and C. Gignoux, Eur. Phys. J. A **13**, 363 (2002) [hep-ph/0101112].

[41] H. Q. Zhou, R. G. Ping and B. S. Zou, Phys. Lett. B **611**, 123 (2005) [hep-ph/0412221].

[42] J. Lu, W. -Z. Deng, X. -L. Chen and S. -L. Zhu, Phys. Rev. D **73**, 054012 (2006) [hep-ph/0602167].

[43] B. Zhang, X. Liu, W. Z. Deng and S. L. Zhu, Eur. Phys. J. C **50**, 617 (2007) [hep-ph/0609013].

[44] Z. -G. Luo, X. -L. Chen and X. Liu, Phys. Rev. D **79**, 074020 (2009) [arXiv:0901.0505 [hep-ph]].

[45] Z. F. Sun and X. Liu, Phys. Rev. D **80**, 074037 (2009) [arXiv:0909.1658 [hep-ph]].

[46] X. Liu, Z. G. Luo and Z. F. Sun, Phys. Rev. Lett. **104**, 122001 (2010) [arXiv:0911.3694 [hep-ph]].

[47] Z. F. Sun, J. S. Yu, X. Liu and T. Matsuki, Phys. Rev. D **82**, 111501 (2010) [arXiv:1008.3120 [hep-ph]].

[48] T. A. Rijken, M. M. Nagels and Y. Yamamoto, Nucl. Phys. A **835**, 160 (2010).

[49] C. -Q. Pang, L. -P. He, X. Liu and T. Matsuki, Phys. Rev. D **90**, 014001 (2014) [arXiv:1405.3189 [hep-ph]].

[50] B. Wang, C. Q. Pang, X. Liu and T. Matsuki, arXiv:1410.3930 [hep-ph].

[51] Z. -C. Ye, X. Wang, X. Liu and Q. Zhao, Phys. Rev. D **86**, 054025 (2012) [arXiv:1206.0097 [hep-ph]].

[52] X. Wang, Z. F. Sun, D. Y. Chen, X. Liu and T. Matsuki, Phys. Rev. D **85**, 074024 (2012) [arXiv:1202.4139 [hep-ph]].

[53] L. -P. He, X. Wang and X. Liu, Phys. Rev. D **88**, 034008 (2013) [arXiv:1306.5562 [hep-ph]].

[54] Y. Sun, X. Liu and T. Matsuki, Phys. Rev. D **88**, 094020 (2013)

[arXiv:1309.2203 [hep-ph]].
[55] E. van Beveren, C. Dullemond and G. Rupp, Phys. Rev. D **21**, 772 (1980) [Erratum-ibid. D **22**, 787 (1980)].
[56] E. van Beveren, G. Rupp, T. A. Rijken and C. Dullemond, Phys. Rev. D **27**, 1527 (1983).
[57] S. Capstick and W. Roberts, Phys. Rev. D **49**, 4570 (1994) [nucl-th/9310030].
[58] P. R. Page, Nucl. Phys. B **446**, 189 (1995) [hep-ph/9502204].
[59] A. I. Titov, T. I. Gulamov and B. Kampfer, Phys. Rev. D **53**, 3770 (1996).
[60] M. Jacob and G. C. Wick, Annals Phys. **7**, 404 (1959) [Annals Phys. **281**, 774 (2000)].
[61] J. -S. Yu, Z. -F. Sun, X. Liu and Q. Zhao, Phys. Rev. D **83**, 114007 (2011) [arXiv:1104.3064 [hep-ph]].
[62] R. R. Akhmetshin *et al.* [CMD2 Collaboration], Phys. Lett. B **466**, 392 (1999) [hep-ex/9904024].
[63] P. Weidenauer *et al.* [ASTERIX. Collaboration], Z. Phys. C **59**, 387 (1993).
[64] F. E. Close and A. Kirk, Z. Phys. C **76**, 469 (1997) [hep-ph/9706543].
[65] R. Aaij *et al.* [LHCb Collaboration], Phys. Rev. Lett. **112**, no. 9, 091802 (2014) [arXiv:1310.2145 [hep-ex]].
[66] J. J. Dudek, R. G. Edwards, P. Guo and C. E. Thomas, Phys. Rev. D **88**, no. 9, 094505 (2013) [arXiv:1309.2608 [hep-lat]].
[67] J. H. Lee, S. U. Chung, H. G. Kirk, D. P. Weygand, H. J. Willutzki, R. Crittenden, A. Dzierba and P. Smith *et al.*, Phys. Lett. B **323**, 227 (1994).
[68] J. E. Augustin *et al.* [DM2 Collaboration], Phys. Rev. D **46**, 1951 (1992).
[69] H. Aihara *et al.* [TPC/Two Gamma Collaboration], Phys. Rev. D **38**, 1 (1988).
[70] H. Y. Cheng, Phys. Lett. B **707**, 116 (2012) [arXiv:1110.2249 [hep-ph]].
[71] J. J. Dudek, R. G. Edwards, B. Joo, M. J. Peardon, D. G. Richards and C. E. Thomas, Phys. Rev. D **83**, 111502 (2011) [arXiv:1102.4299 [hep-lat]].
[72] D. M. Li, B. Ma and H. Yu, Eur. Phys. J. A **26**, 141 (2005) [hep-ph/0509215].
[73] A. V. Anisovich, C. A. Baker, C. J. Batty, D. V. Bugg, V. A. Nikonov, A. V. Sarantsev, V. V. Sarantsev and B. S. Zou, Phys. Lett. B **507**, 23 (2001).